Functional analysis of FSP27 protein regions for lipid droplet localization, caspase-dependent apoptosis, and dimerization with CIDEA

Kun Liu, Shengli Zhou, Ji-Young Kim, Kristin Tillison, David Majors, David Rearick, Jun Ho Lee, Ruby F. Fernandez-Boyanapalli, Katherine Barricklow, M. Sue Houston and Cynthia M. Smas

Am J Physiol Endocrinol Metab 297:E1395-E1413, 2009. First published 20 October 2009; doi:10.1152/ajpendo.00188.2009

Am J Physiol Endocrinol Metab 297: E1395–E1413, 2009.
First published October 20, 2009; doi:10.1152/ajpendo.00188.2009.

Functional analysis of FSP27 protein regions for lipid droplet localization, caspase-dependent apoptosis, and dimerization with CIDEA

Kun Liu,[1]* Shengli Zhou,[1]* Ji-Young Kim,[1] Kristin Tillison,[1] David Majors,[1] David Rearick,[1] Jun Ho Lee,[1] Ruby F. Fernandez-Boyanapalli,[1] Katherine Barricklow,[2] M. Sue Houston,[2] and Cynthia M. Smas[1]

[1]*Department of Biochemistry and Cancer Biology and Center for Diabetes and Endocrine Research; The University of Toledo College of Medicine, Toledo; and* [2]*Food and Nutrition Program School of Family and Consumer Sciences, Bowling Green State University, Bowling Green, Ohio*

Submitted 20 March 2009; accepted in final form 13 October 2009

Liu K, Zhou S, Kim J, Tillison K, Majors D, Rearick D, Lee JH, Fernandez-Boyanapalli RF, Barricklow K, Houston MS, Smas CM. Functional analysis of FSP27 protein regions for lipid droplet localization, caspase-dependent apoptosis, and dimerization with CIDEA. *Am J Physiol Endocrinol Metab* 297: E1395–E1413, 2009. First published October 20, 2009; doi:10.1152/ajpendo.00188.2009.— The adipocyte-specific protein FSP27, also known as CIDEC, is one of three cell death-inducing DFF45-like effector (CIDE) proteins. The first known function for CIDEs was promotion of apoptosis upon ectopic expression in mammalian cells. Recent studies in endogenous settings demonstrated key roles for CIDEs in energy metabolism. FSP27 is a lipid droplet-associated protein whose heterologous expression enhances formation of enlarged lipid droplets and is required for unilocular lipid droplets typical of white adipocytes in vivo. Here, we delineate relationships between apoptotic function and lipid droplet localization of FSP27. We demonstrate that ectopic expression of FSP27 induces enlarged lipid droplets in multiple human cell lines, which is indicative that its mechanism involves ubiquitously present, rather than adipocyte-specific, cellular machinery. Furthermore, promotion of lipid droplet formation in HeLa cells via culture in exogenous oleic acid offsets FSP27-mediated apoptosis. Using transient cotransfections and analysis of lipid droplets in HeLa cells stably expressing FSP27, we show that FSP27 does not protect lipid droplets from action of ATGL lipase. Domain mapping with eGFP-FSP27 deletion constructs indicates that lipid droplet localization of FSP27 requires amino acids 174–192 of its CIDE C domain. The apoptotic mechanism of FSP27, which we show involves caspase-9 and mitochondrial cytochrome *c*, also requires this 19-amino acid region. Interaction assays determine the FSP27 CIDE C domain complexes with CIDEA, and Western blot reveals that FSP27 protein levels are reduced by coexpression of CIDEA. Overall, our findings demonstrate the function of the FSP27 CIDE C domain and/or regions thereof for apoptosis, lipid droplet localization, and CIDEA interaction.

fat-specific protein 27; cell death-inducing DFF45-like effector A; adipose

OBESITY AND ITS RELATED COMORBIDITIES are approaching epidemic levels (1, 9). The development of new therapeutic inroads to treat these conditions would be greatly facilitated by a full understanding of lipid homeostasis (35, 36). Lipotoxicity is a highly detrimental outcome of the obese state, leading to derangement of cell function and/or cell death in various tissues (34, 35, 37). White adipocytes present in white adipose tissue are the major site storage of excess energy in the form of triacylglycerol, contained within intracellular lipid droplets (7, 38). Efficient storage of excess fatty acids within adipocyte lipid droplets also serves to protect other cells and tissues from their lipotoxic effects (7, 38). Lipid droplets are highly dynamic organelles consisting of a neutral lipid core, a phospholipid monolayer, and a large number of lipid droplet-associated proteins (7, 38). The role for the vast majority of these proteins in lipid droplet function is undetermined. Although most cells of the body are thought to contain small lipid droplets that serve to sequester fatty acids and meet ongoing energy needs, the white adipocyte is unique in that nearly all of its cell volume is filled by a large unilocular lipid droplet.

The cell death-inducing DFF45-like effector (CIDE) protein family consists of three ~22- to 27-kDa proteins: fat-specific protein 27 (FSP27; also known as CIDEC), CIDEA, and CIDEB; each are newly recognized lipid droplet-associated proteins with key roles in lipid homeostasis and energy balance (14–16, 21, 26, 41, 42). Curiously, the first described function of CIDEs was promotion of apoptosis. FSP27, CIDEA, and CIDEB exert robust apoptotic activity upon ectopic expression in mammalian cells (5, 8, 11, 13, 17). CIDE proteins have a region of amino acid sequence homology in their NH_2-terminal halves, termed the CIDE N domain, that is also present in the major proapoptotic nuclease DFF40 and its inhibitory partner protein DFF45 (11). A CIDE C domain, present in their COOH-terminal halves, is found only in FSP27, CIDEA, and CIDEB (11). Although the physiological role of CIDE-induced apoptosis remains undetermined, recent studies for FSP27, CIDEA, and CIDEB have greatly illuminated the role of endogenous CIDE proteins and indicate that they have crucial roles in lipid metabolism (14–16, 24, 33, 42, 44). Gene knockout has demonstrated that FSP27 is requisite for formation of the unilocular lipid droplet that typifies white adipocytes in vivo. In vitro knockdown of FSP27 in adipocytes results in an apparent fragmentation and/or a failed fusion of lipid droplets that results in cells with many markedly smaller lipid droplets, and such cells show evidence of enhanced lipolysis (21, 24). FSP27 and CIDEA are expressed only in adipocytes, with distinctions noted for transcript expression in human vs. mouse. FSP27 transcript is expressed in both human and murine white adipocytes (13, 25) and is present at lower levels in murine brown adipocytes (13). In mice, CIDEA is found only in brown adipocytes (13, 44), whereas in humans a high level of CIDEA is noted in white adipocytes (26). CIDEB transcript is markedly enriched in human and murine liver,

* These authors contributed equally to this work.

Address for reprint requests and other correspondence: C. M. Smas, Dept. of Biochemistry and Cancer Biology and Center for Diabetes and Endocrine Research, Univ. of Toledo College of Medicine, Toledo, OH 43614 (e-mail: cynthia.smas@utoledo.edu).

with expression also reported for murine kidney and intestine (11, 13, 15).

Earlier reports described a mitochondrial localization for FSP27, CIDEA, and CIDEB (5, 17, 44). However, recent studies strongly suggest that this localization was incorrect and that FSP27, CIDEA, and CIDEB are lipid droplet-associated proteins (12, 21, 25, 33, 42). Signal for an FSP27-enhanced green fluorescent protein (eGFP) fusion protein has been shown to be colocalized to lipid droplets in 3T3-L1 adipocytes and lipid-loaded 293T cells (12). Immunostaining for endogenous or ectopically expressed FSP27 localized it to lipid droplets of 3T3-L1 adipocytes and cultured human white adipocytes (21, 25). Ectopically expressed CIDEA-eGFP localized to lipid droplets in 3T3-L1 adipocytes and COS cells and endogenous CIDEA protein is found at lipid droplets of cultured human white adipocytes and cultured murine brown adipocytes (26). Most recently, ectopically expressed CIDEB was shown to be localized to lipid droplets of lipid-loaded hepatocytes and the regions of the CIDEB protein that governed lipid droplet localization examined (42). Ectopic expression of an HA-tagged or eGFP fusion construct containing amino acids 166–195 of CIDEB was sufficient for lipid droplet targeting in lipid-loaded COS cells and HepG2 hepatocytes, respectively (42). CIDEA and CIDEB are also reportedly localized to the endoplasmic reticulum, an organelle from which biogenesis of intracellular lipid droplets initiates (27, 42). Moreover, in addition to being lipid droplet-localized proteins per se, ectopic expression of FSP27 and CIDEA has been demonstrated to promote the formation and/or enlargement of lipid droplets in several nonadipocyte cell types, a phenomenon that is particularly evident with addition of exogenous oleic acid to culture media. This has been shown for FLAG-tagged FSP27 in 3T3-L1 preadipocytes (12) and for eGFP-FSP27 in 3T3-L1 preadipocytes, 293T, and COS cells (12, 25). For CIDEA, FLAG-tagged CIDEA has been demonstrated to promote lipid droplet formation in 3T3-L1 preadipocytes (12). eGFP-CIDEA has been reported to enhance lipid droplet size in lipid-loaded 3T3-L1 preadipocytes and lipid-loaded COS cells (26). On the other hand, FSP27 knockdown reduced the size and increased the number of smaller lipid droplets in 3T3-L1 adipocytes (12, 25) and human adipocytes (21).

Analysis of FSP27-null mice indicates that FSP27 facilitates efficient energy storage in white adipose tissue (WAT) by promoting formation of unilocular lipid droplets to restrict lipolysis (21). FSP27-null mice are refractory to diet-induced obesity and insulin resistance (21, 24, 33). They have markedly reduced WAT mass that shows evidence of some features of brown adipose tissue (BAT), including increased mitochondrial biogenesis and enhanced β-oxidation, with FSP27-null white adipocytes containing smaller, multilocular lipid droplets (21, 33). On the other hand, transgenic expression of FSP27 in murine liver results in hepatosteatosis (20). CIDEA-null mice exhibit elevated lipolysis in BAT and resist diet-induced obesity (44). A recent report demonstrated that one mechanism of CIDEA action is via its interaction with the major metabolic regulator AMP-activated protein kinase (AMPK), which reduces AMPK protein level by enhancing proteosome-mediated AMPK degradation (27). The phenotype of CIDEA-null mice was attributed initially to the ability of CIDEA to regulate thermogenesis via interaction with uncoupling protein-1 (UCP1) to inhibit UCP1 activity (44). Given that the initial mitochondrial localization reported for CIDEA appears to not be the case (27), CIDEA interaction with UCP1 remains to be fully clarified. CIDEB interacts with apolipoprotein B and promotes the formation of triacylglycerol-enriched VLDL particles (42). CIDEB-null mice display decreased plasma triglycerides and free fatty acids and are refractory to diet-induced obesity (15). Livers of CIDEB-null mice have higher levels of triacylglycerols and lower VLDL secretion, with VLDL containing less triacylglycerol (42). Studies in humans have reported that the levels of FSP27 and CIDEA transcript are higher in the WAT of obese insulin-sensitive persons compared with WAT of obese insulin-resistant persons. This indicates a possible positive protective effect of elevated WAT FSP27 and CIDEA expression in the relationship between fat mass and the detrimental impact of obesity on systemic metabolism in humans (25, 26). Additionally, partial lipodystrophy, alteration in WAT morphology to multilocular lipid droplets, and insulin-resistant diabetes have recently been reported for a patient with a homozygous nonsense mutation in FSP27/CIDEC that generates a truncated protein form largely lacking the CIDE C domain (30a).

Taken together, studies to date indicate that endogenous FSP27 protein has a primary role in lipid droplet formation and energy balance. On the other hand, when FSP27 is expressed outside of the lipid droplet context, it manifests proapoptotic activity. In this report, we provide a detailed examination of the apoptotic mechanisms of FSP27 action and conduct structure-function analysis of FSP27 in regard to regions of the protein involved in lipid droplet localization, apoptotic response, and interaction with CIDEA.

MATERIALS AND METHODS

Cell culture and cotransfection-based assessment of cell death. All cell lines were maintained in DMEM supplemented with 10% FBS. The pan caspase inhibitor Z-VAD-FMK (R & D Systems, Minneapolis, MN) and the negative control peptide VA-FMK (BD Biosciences, San Jose, CA) were used at 20 μM and added to cultures at the time of transfection. All transfections were carried out using Lipofectamine 2000 (Invitrogen, Carlsbad, CA). For studies using combinations of expression constructs for FSP27 and dominant-negative caspase-9 (CS9DN), DNAs were cotransfected at the indicated mass ratios of plasmids and assessed at 48 h posttransfection. We utilized a β-galactosidase cotransfection assay as an indirect visual measurement of cell death; this protocol has been described in previous studies of apoptosis (6, 13). The β-galactosidase construct serves as a reporter to mark transfected cells, which are also cotransfected with a test "effector" plasmid(s), e.g., FSP27 or empty vector (EV) pcDNA3.1. Cells that die are lost from cultures and therefore not counted among the LacZ+ blue cells. Comparison of the numbers of blue cells in cultures transfected with EV vs. those transfected with the effector plasmid(s) allow for detection of the degree of cell death. For experiments involving enumeration of β-galactosidase (LacZ) positive cells, cotransfections included 10 ng of a β-galactosidase expression construct. Transfections were done in triplicate, and unless stated otherwise, blue cells were counted at 48 h. For β-galactosidase staining, cells were fixed for 5 min at room temperature in 0.5% glutaraldehyde in PBS. Following two PBS washes, cells were incubated in staining solution [2 mM $MgCl_2$, 5 mM $K_3Fe(CN)_6$, 5 mM $K_4Fe(CN)_6$, 1 mg/ml 5-bromo-4-chloro-3-indolyl-β-D-galactopyranoside in PBS] and incubated at 37°C for 4 h. After incubation, blue cells per microscopic field were enumerated with 10 independent

randomly chosen fields analyzed/dish or well. Single-factor ANOVA was used for statistical assessments.

Assessment of DNA fragmentation. Genomic DNA was prepared either with the use of an Apoptotic DNA Ladder Kit (Roche Diagnostics, Nutley, NJ) exactly per the manufacturer's directions or by manual preparation using standard methods. For the latter, cells were collected from the media and culture plates and subjected to low-speed centrifugation. The pellet was resuspended in lysis buffer (20 mM EDTA, 5 mM Tris·HCl, pH 8.0, 0.5% SDS) and incubated on ice for 20 min. Insoluble material was removed by centrifugation and the supernatant extracted with phenol-chloroform. DNA was ethanol precipitated and the pellet resuspended in water and subjected to RNase digestion. DNA was assessed by fractionation on 1.2% agarose gels, stained with ethidium bromide or SYBR green, visualized under UV illumination, and photographed. All images shown accurately represent the original data; however, minor adjustments to brightness and contrast were made to allow for better visualization. Images shown as a single panel in DNA fragmentation assays were run on the same agarose gel. However, in some instances lanes have been removed and/or rearranged for economy and clarity of presentation.

Immunocytochemical staining and Western blot analysis for cytochrome c release. For immunocytochemistry, COS cells were grown overnight on laminin-coated coverslips in six-well plates and transfected with 2 μg of DNA of the indicated eGFP-FSP27 construct or empty eGFP vector. At 20 h posttransfection, cells were fixed with cold methanol for 10 min. Coverslips were blocked by incubation in 0.1% BSA in PBS for 30 min and incubated at room temperature with monoclonal antibody for cytochrome *c*. Coverslips were washed three times for 3 min each with 0.1% BSA in PBS. Secondary antibody was Alexa fluor 568-conjugated goat anti-mouse. After three 3-min washes with 0.1% BSA in PBS, nuclei were stained with 10 nM 4,6-diamidino-2-phenylindole (DAPI) for 10 min, coverslips were mounted on glass slides, and images were obtained. Negative controls showed no signals and consisted of eGFP EV transfectants and immunocytochemical staining of eGFP-FSP27 transfectants with secondary antibody only. Signals were documented using a Nikon Eclipse E800 fluorescence microscope equipped with a digital camera and image acquisition, and merging was performed with Image-Pro Plus software (Media Cybernetics, Carlsbad, CA) or with an Olympus IX70 microscope using Spot Advanced software (Diagnostic Instruments, Sterling Heights, MI). All images shown accurately represent the original data; however, minor adjustments to brightness and contrast were made to allow for better visualization. Similar observations were observed in multiple microscopic fields and in duplicate studies, with representative data presented.

For Western blot studies of cytochrome *c* release, COS cells were collected at 18 h posttransfection. Cytosolic fraction was prepared using a Mitosciences Cell Fractionation Kit exactly per the manufacturer's instructions. Transfections and protein preparations were conducted in triplicate. Western blots were carried out using a 1:5,000 dilution of anti-cytochrome *c* antibody (MSA06; Mitosciences) and a 1:2,000 dilution of secondary antibody (SC-2005; Santa Cruz Biotechnology). GAPDH monoclonal primary antibody was used at 1:10,000 (SC-47724; Santa Cruz Biotechnology), and monoclonal ATP synthase-α primary antibody was used at 1:1,000 (MS507; Mitosciences). Antibody incubations were carried out for 1 h at room temperature. Blocking, washing, and enhanced chemiluminescence are described in *Other Western blot analysis and coimmunoprecipitation* (below). Digital images were obtained and data quantified using FluorChem HD2 software and an Alpha Innotech Digital imaging system. Statistical analysis was by single-factor ANOVA.

Other Western blot analysis and coimmunoprecipitation. For all other Western blot studies, exclusive of cytochrome *c* studies, cell lysates were harvested at 48 h posttransfection by lysis in TNN(+) buffer (10 mM Tris, pH 8.0, 120 mM NaCl, 0.5% NP-40, 1 mM EDTA supplemented with a protease inhibitor cocktail). Lysates were incubated on ice for 30 min with intermittent vortexing, the supernatant was collected via centrifugation, and protein content was determined (Bio-Rad, Hercules, CA). For coimmunoprecipitation experiments, 500 μg of protein extract was incubated with 20 μl of anti-FLAG M2-agarose affinity gel (Sigma-Aldrich, Minneapolis, MN) and coimmunoprecipitation performed per the manufacturer's directions. For analysis of protein half-life, cells were treated with 100 ng/ml cycloheximide at 40 h posttransfection. For Western blot analyses, typically, 50 μg of protein extract was fractionated on SDS-PAGE, followed by electroblotting onto PVDF membrane with 0.025 M Tris-0.192 M glycine transfer buffer supplemented with 20% methanol. Membranes were blocked for 1 h in 5% nonfat milk in PBS-T followed by either 1 h of incubation at room temperature, or overnight at 4°C, with a 1:2,000 dilution of antibody to full-length p116 poly-ADP-ribose polymerase (PARP), cleaved p89 PARP, cleaved p150 α-fodrin, cleaved p37 caspase-9, cleaved p20 caspase-7, cleaved p19 caspase-3 (Cell Signaling Technology, Beverley, MA), or eGFP antibody (Covance Research Products, Berkeley, CA). Secondary antibody was horseradish peroxidase-conjugated goat anti-rabbit (Bio-Rad) used at a 1:2,000 dilution. All washes were conducted in PBS-T. Signal was detected by ECL Plus enhanced chemiluminescence (GE Healthcare, Waukesha, WI) and exposure to X-ray film or the use of a FluorChem HD2 digital imaging system (Alpha Innotech, San Leandro, CA). Signal intensity was quantified using AlphaEaseFC software (Alpha Innotech, San Leandro CA). For protein half-life studies, relative signal intensity was normalized to the *time 0* time point, which was set to 100%. Excel software was used to generate a line-fitting equation and half-life calculated. All images shown accurately represent the original data; however, minor adjustments to brightness and contrast were made to allow for better visualization. Images shown in the same horizontal Western blot panel were run on the same gel and processed on the same membrane. However, in some instances lanes have been removed and/or rearranged for economy and clarity of presentation.

Lipid droplet subcellular localization and lipid droplet formation studies. Expression constructs for native full-length FSP27, CIDEA, CIDEB, and adipose triglyceride lipase (ATGL) contained the complete open reading frame. Expression constructs for eGFP full-length FSP27, CIDEA, and CIDEB, DSRed-CIDEA, or eGFP CIDE C or CIDE N of FSP27 lacked the respective initiator methionine and were generated by PCR-based cloning using sequence-verified IMAGE cDNA clones as template. The FSP27-N constructs contained amino acids 1–140 and the FSP27-C constructs amino acids 118–238. For eGFP constructs of Δ173-FSP27 and Δ192-FSP27, an Erase-A-Base kit (Promega, Madison, WI) was employed according to the manufacturer's instructions. For the FSP27-pBABE-puro construct, the open reading frame of FSP27 was cloned by PCR into the pBABE-puro vector. All constructs were confirmed by full sequencing of inserts.

For lipid droplet localization studies, HeLa cells were grown for 3 days in DMEM with 10% FCS supplemented with 400 μM BSA-complexed oleic acid to induce lipid droplet formation. Cells were then transfected with the indicated expression construct or corresponding EV. During transfection, DNA complexes were incubated with cells for 6 h in the absence of exogenous oleic acid, after which medium was changed to DMEM with 10% FCS and 400 μM BSA-complexed oleic acid. At 16 h posttransfection, lipid droplets were stained with Nile Red by incubating cells for 15 min with 0.5 μg/ml Nile red (Invitrogen). Confocal documentation of eGFP and Nile red signals in live cells transfected with eGFP-FSP27 or regions thereof used the resources of the Advanced Microscopy and Imaging Center at the University of Toledo Health Science Campus. Images were captured with a Leica TCS SP5 broadband confocal microscope (Leica, Mannheim, Germany) equipped with Argon-488 and diode-pumped solid-state-561 laser sources and 63.0 × 1.40 NA oil immersion objective. A series of optical Z sections, 0.5 μM in thickness and totaling 5–6 μM, were collected and visualized as projection images using Leica LAS software. Laser intensities and microscope settings

between samples were maintained constant. Other imaging studies of lipid droplet localization used an Olympus IX70 microscope using Spot Advanced software (Diagnostic Instruments).

For transient transfection studies of the effects of FSP27, CIDEA, or CIDEB on lipid droplet formation across multiple cell lines, cells were used without preculture in exogenous oleic acid. HeLa, HT1080, ZR75, LNCaP, MG63, or U2OS cells were transfected with expression constructs for nontagged native versions of FSP27, CIDEA, or CIDEB in pcDNA3.1 or empty pcDNA3.1 vector, as indicated. Medium was supplemented with 400 μM BSA-complexed oleic acid at 4 h posttransfection. Cells were documented at 18 h posttransfection by fixation in 4% formalin and staining with Oil Red O. For studies of effects of ATGL expression by transient cotransfection with FSP27, HeLa cells were transfected with a 1:5 mass ratio of expression construct for FSP27 and ATGL in pcDNA3.1 or FSP27 and EV (pcDNA3.1). At 4 h posttransfection, medium was changed to include 400 μM of BSA-complexed oleic acid. Studies using ATGL expressed from the vector pIRES2-eGFP (pIRES2-eGFP-ATGL), wherein cells transfected with ATGL could be tracked on the basis of green signal, were conducted in a similar manner, except in this case a 5:1 ratio of FSP27 and ATGL constructs was used. Cells were analyzed at 12–16 h posttransfection for lipid content by photography, cell counting, and flow cytometry (described below). Cell counting and flow cytometry studies were carried out in triplicate. Statistical analysis was by single-factor ANOVA. For cell-counting studies wherein ATGL was expressed from pcDNA3.1, the number of cells with large lipid droplets per microscopic field were enumerated. For cell-counting studies wherein ATGL was expressed as pIRES2-eGFP-ATGL, green cells per field were scored for the presence of large lipid droplets. For both of these counting studies, unstained live cells were examined with 10 individual fields analyzed per each of triplicate transfections, with a minimum of 100 cells analyzed/replicate. Data were expressed as a percent of cells, or green cells in the case of pIRES2-eGFP-ATGL, with lipid droplets.

For studies of the effects of ATGL on preformed FSP27-induced lipid droplets, we prepared stable cell populations of HeLa cells expressing FSP27 via retroviral infection of a FSP27-pBABE-puro construct, with cells infected with EV pBABE-puro as a control population. Cells surviving following selection in 2 μg/ml puromycin were pooled for analysis. For assessment of ATGL effects, we conducted studies using ATGL expressed in pcDNA3.1 and studies using pIRES2-eGFP-ATGL. In either case, HeLa-FSP27 cells were pretreated with BSA-complexed 400 μM oleic acid for 1 or 3 days to induce lipid droplet formation and then transiently transfected with either an ATGL expression construct (in pcDNA3.1 or in pIRES2-eGFP) or corresponding EV. Cells were analyzed at 12–16 h posttransfection for lipid content by photography, cell counting, and flow cytometry (described below). Cell counting and flow cytometry studies were carried out on quadruplicate transfected samples. For cell-counting studies wherein ATGL was expressed from pcDNA3.1, the number of cells with large lipid droplets per microscopic field was enumerated, with at least five individual fields analyzed per each of quadruplicate transfections and at least 100 cells scored for each replicate. For cell-counting studies employing pIRES2-eGFP-ATGL, green cells per field were scored for the presence of large lipid droplets, with at least 10 fields and 100 total green cells analyzed per replicate. For both of these counting studies, unstained live cells were examined. Data were expressed as a percent of cells, or green cells in the case of pIRES2-eGFP-ATGL, with evident lipid droplets.

For photographic documentation of lipid droplet formation, live cells were stained for neutral lipid with either Bodipy 493/503 (D-3922; Molecular Probes) or LipidTox Deep Red (H34477; Invitrogen). For this, cells on tissue culture plates were rinsed with PBS and stained for 10 min with 5 μM Bodipy 493/503 or a 1:2,000 dilution of LipidTox Deep Red in PBS. Staining and incubations were at 37°C. After staining, cells were washed once with PBS, followed by a 10-min incubation in PBS; this was then replaced with fresh PBS. Digital images were obtained with an Olympus IX70 microscope using Spot Advanced software (Diagnostic Instruments). All images shown accurately represent the original data; however, minor adjustments to brightness and contrast were made to allow for better visualization. Similar observations were observed in multiple microscopic fields and in duplicate studies, with representative data presented.

For flow cytometry analysis of neutral lipid content per cell, cells were stained with LipidTox Deep Red or Bodipy 493/503, as described above for photographic imaging. Cells were then trypsinized, washed with medium in suspension, pelleted with low-speed centrifugation, and resuspended in PBS. For each study, 10,000 cells of independent quadruplicate transfections were analyzed using a BD Biosciences FACSCalibur flow cytometer using the Flow Cytometry Core Facility of the University of Toledo College of Medicine.

Yeast two-hybrid assessment of protein-protein interactions. Coding sequences for full-length FSP27, the CIDE N or CIDE C domains of FSP27, or full-length CIDEA were generated by PCR-based cloning and inserted into the *Eco*RI and *Bam*HI sites of pGBKT7 to produce Gal4 DNA binding fusion constructs and of pGADT7 to produce the Gal4 activation domain fusion constructs. Reading frame across the vector-insert junction and the insert was fully sequence verified. The indicated pairwise combinations of activation domain fusion and binding domain fusion constructs were cotransformed into *S. cerevisiae* yeast strain AH109. Cotransformants were selected following incubation for 4 days at 30°C on Leu and Trp double-dropout (DDO) media. Colonies from each pairwise cotransformation were patched onto DDO media plates, His, Leu, and Trp triple-dropout (TDO) media plates, and TDO media plates containing the chromogenic substrate X-α-galactosidase. After 4 days of growth at 30°C, growth patterns were assessed and digital images generated. All images shown accurately represent the original data; however, minor adjustments to brightness and contrast were made to allow for better visualization. Images shown in a boxed area arose from the same agar plate. However, in some instances lanes have been removed and/or rearranged for economy and clarity of presentation.

RESULTS AND DISCUSSION

FSP27, CIDEA, and CIDEB promote lipid droplet formation in multiple cell types. To date, ectopic expression of FSP27 protein has been tested for promotion of formation of enlarged lipid droplets in several nonadipocyte cell types. To further address the range of cell types wherein FSP27 and CIDEA can exert a lipid droplet enlargement phenotype, we tested the effects of transient expression of FSP27, CIDEA, or EV on six human cancer cell lines of various cellular origins, including cervical cancer (HeLa), fibrosarcoma (HT1080), breast cancer (ZR75), prostate cancer (LNCaP), and osteosarcoma (MG63, U2OS; Fig. 1*A*). At 4 h posttransfection, culture medium was supplemented with 400 μM oleic acid and intracellular lipid stained with Oil Red O 14 h later. Transfection of pcDNA3.1 EV resulted in accumulation of multiple tiny lipid deposits/droplets in oleic acid-treated cells. In contrast, expression of FSP27 or CIDEA resulted in the robust accumulation of visibly enlarged lipid droplets that were first observed at ~10 h posttransfection. The lipid droplet enlargement phenotype was observed in each of the six cell lines tested. We also noted that the appearance of enlarged lipid droplets was concomitant with the disappearance of the tiny lipid deposits/droplets from within the same cell, suggestive that FSP27 and CIDEA proteins may act by mediating fusion of tiny lipid deposits/droplets to generate much larger lipid droplets. CIDEB was recently described as a lipid droplet-associated protein in hepatocytes (42), one of several tissues that express high levels

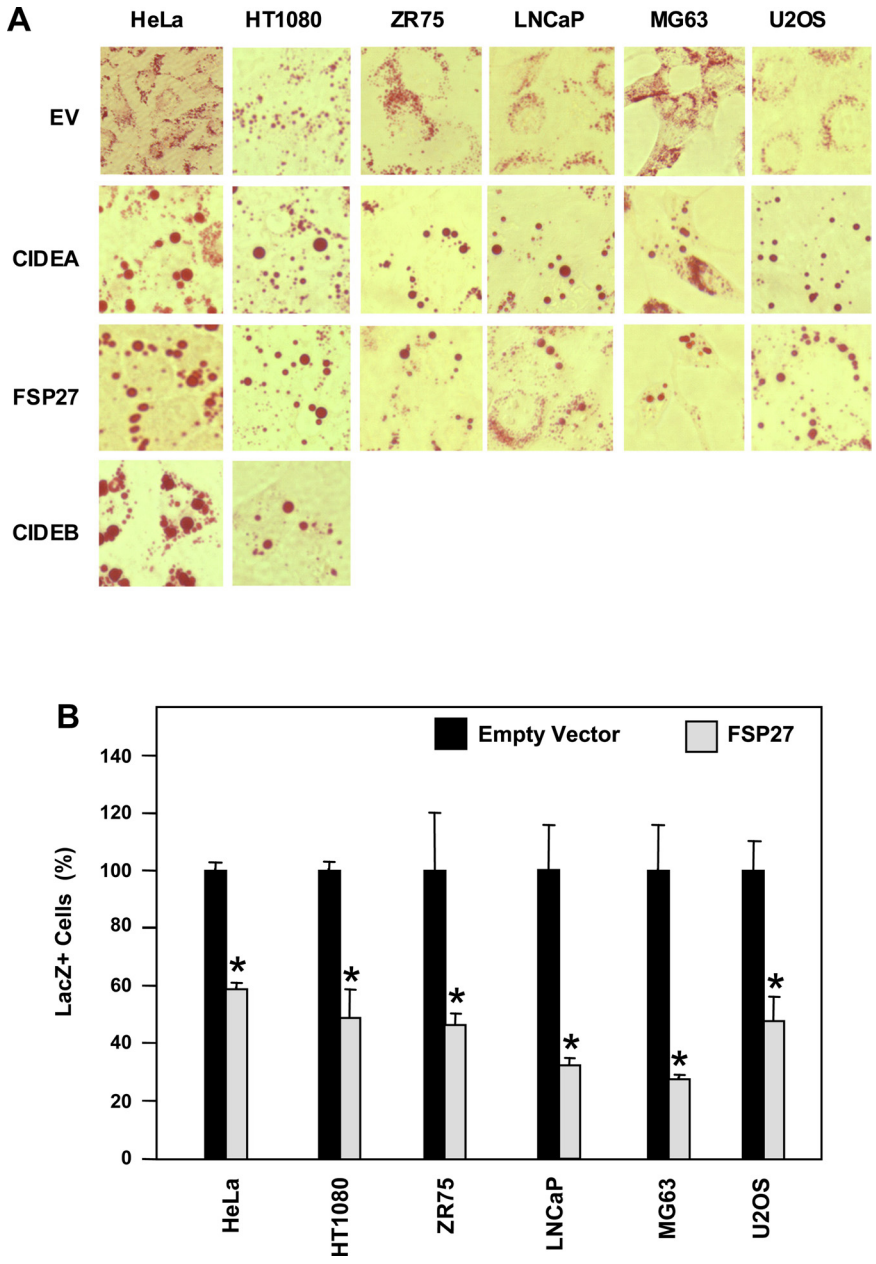

Fig. 1. Fat-specific protein 27 (FSP27) promotes lipid droplet formation and apoptosis across multiple cell lines. *A*: promotion of lipid droplet formation by cell death-inducing DFF45-like effector (CIDE) proteins. The indicated cell lines were transfected with either empty vector (EV), CIDEA, FSP27, or CIDEB. Cells were switched to culture media supplemented with 400 μM BSA-complexed oleic acid at 4 h posttransfection and the next day stained with Oil Red O. *B*: FSP27 induces apoptosis in multiple cell types. Cells were transfected with an empty vector or an FSP27 expression construct along with a marker β-galactosidase expression construct, as described in MATERIALS AND METHODS. At 24 h posttransfection, the numbers of β-galactosidase (LacZ+) cells were enumerated, with that for empty vector transfectants set to 100% for each respective cell line. Data are shown as means ± SD. $*P < 0.01$.

of endogenous CIDEB transcript. Although CIDEB has been shown to function in VLDL synthesis (42), the ability of ectopic CIDEB to promote lipid droplet formation in heterologous cell types (i.e., nonhepatocytes) has not been addressed. Because the focus of our study was on the two CIDE proteins present in adipocytes, FSP27 and CIDEA, we assessed the lipid droplet-promoting effects of CIDEB in only two cell lines, HeLa and HT1080. However, our data suggest that, like CIDEA and FSP27, CIDEB also possesses a robust lipid droplet formation/enlargement activity. Overall, these observations point to the likely ability of FSP27 and CIDEA to promote formation of enlarged lipid droplets in most, and possibly all, cell types. This underscores the notion that their mechanisms of action in lipid droplet formation utilize cellular machinery generally present in many cell types rather than pathways and factors specific to adipocytes or other sites of endogenous CIDE protein expression. On the other hand, in the course of our studies with FSP27, we never observed lipid droplets of the strikingly large and unilocular morphology that characterize white fat cells in vivo in our studies with FSP27, suggesting that additional and possibly adipocyte-specific proteins are needed for such.

To date, two apparently disparate roles have been demonstrated for CIDE proteins, lipid droplet function and proapoptotic function. Recent in vitro and in vivo studies demonstrate a key role for FSP27 in lipid metabolism and support the idea that the primary function for endogenous FSP27 in vivo is the formation of large unilocular lipid droplets in adipocytes (21, 33). In the presence of oleic acid supplementation of media, we show herein that FSP27 promotes efficient packaging of triacylglycerol into enlarged lipid droplets in multiple cell types. On the other hand, in the same cell types, cell death ensues

upon heterologous CIDE protein expression under standard culture conditions (i.e., lacking exogenous oleic acid supplementation). This is illustrated by the fact that, for each of the cell lines examined in Fig. 1*A* for the ability of FSP27 to promote lipid droplet formation, expression of FSP27 in the absence of exogenous oleic acid supplementation resulted in cell death (Fig. 1*B*).

Partitioning FSP27 protein into lipid droplets attenuates its apoptotic activity. We have shown previously in studies with 293T cells that the level of ectopically expressed FSP27 transcript is similar to that found in mature fat cells (13). However, despite this high expression level of FSP27 in white adipocytes, we have failed to find evidence of basal apoptosis in 3T3-L1 adipocytes under normal culture conditions (13). This indicates that the induction of FSP27 gene expression that occurs during the normal adipogenic program, and which is concomitant with lipid droplet accumulation, does not result in increased cellular apoptosis. Given that FSP27 is a lipid droplet-associated protein, we postulated that, in the lipid droplet milieu of the adipocyte, FSP27 is unable to exert its apoptotic action. Therefore, we reasoned that, by partitioning FSP27 into lipid droplets, we might be able to attenuate its proapoptotic action.

To test this, we assayed the ability of FSP27 to promote HeLa cell death in the absence and presence of exogenous oleic acid. We first determined the ability of FSP27 to localize to lipid droplets in HeLa cells, as has been reported for a few other nonadipocyte cell types. Confocal analysis in Fig. 2*A* reveals that EV eGFP shows uniformly cytoplasmic signal. On the other hand, there is clear localization of eGFP-FSP27 fusion protein in a discrete ring-like signal at the surface of lipid droplets. The vast majority of visible eGFP-FSP27 signal localizes with staining for intracellular lipid, in some cases to extremely small lipid droplets. Likewise, nearly all of the Nile red signal is coincident with that for eGFP-FSP27, even in areas of the cell where clearly spherical lipid droplets are not yet apparent. We also used confocal analysis to determine localization of CIDEA and CIDEB to HeLa cell lipid droplets. CIDEA had previously been described to localize to lipid droplets in 3T3-L1 adipocytes, and expression of eGFP-CIDEA enhanced lipid droplet formation in two nonadipocyte cell types, 3T3-L1 preadipocytes and COS cells (12, 26). However, it was noted that, in these nonadipose cells, most of the eGFP-CIDEA signal was not colocalized with that for lipid droplets (26) but rather appeared as punctuate signals in the cytoplasm. As such, it was suggested that other likely adipocyte differentiation-dependent proteins are needed to enable a lipid droplet localization for CIDEA (26). The assessments by these investigators were conducted at 24 h posttransfection, with oleic acid added at 8 h posttransfection. Based on our prior experience we have found that, in media that is not supplemented with oleic acid, CIDEs induce robust apoptosis with morphological alterations visible beginning at ~20 h posttransfection (13). Close inspection of

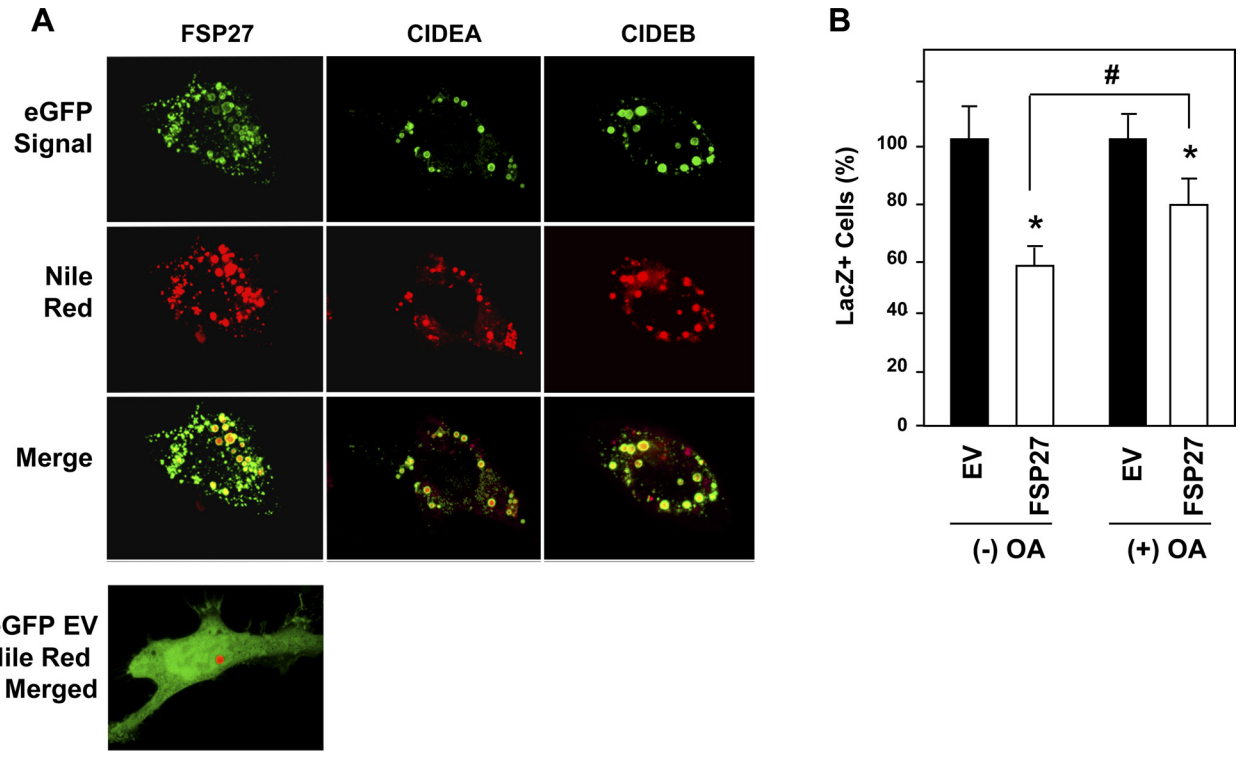

Fig. 2. Localization of FSP27 at lipid droplets attenuates its apoptotic effect. *A*: localization of FSP27 to lipid droplets in HeLa cells. Lipid-loaded HeLa cells were transfected with an enhanced green fluorescent protein (eGFP) expression construct for full-length FSP27, CIDEA, or CIDEB. At 16 posttransfection, live cells were stained with Nile red to visualize lipid droplets and assessed by confocal microscopy. *Top*: eGFP signal; *upper middle*: lipid droplet signal stained with Nile red; *lower middle*: merged image for eGFP and Nile red signal; *bottom*: merged imaged of eGFP EV signal and Nile red signal. *B*: presence of intracellular lipid droplets attenuates FSP27-mediated apoptosis. HeLa cells were cultured for 1 day in the presence or absence of 400 μM BSA-complexed oleic acid (OA) and then transfected with either EV or an FSP27 expression construct, along with a marker LacZ+ expression construct, as described in MATERIALS AND METHODS. LacZ+ blue cells were enumerated 24 h later. The number of cells in the respective EV transfectants was set to 100%. Data are shown as means ± SD. #$P < 0.05$ for FSP27 in absence vs. presence of OA; *$P < 0.05$ vs. respective EV control.

the various cell morphology data presented by Puri et al. (26) suggests that the cells examined for CIDEA expression may have already been undergoing apoptosis. Our data for lipid-loaded HeLa cells in Fig. 2*A*, obtained at ~16 h posttransfection, clearly show that for both CIDEA and CIDEB nearly all of the respective eGFP-CIDE signal localizes to lipid droplets in this nonadipocyte cell type. During the preparation of this article, the lipid droplet localization for CIDEB, which had previously been unknown, was reported (42). This was assessed in CIDEB-null hepatocytes, a cell type that normally expresses CIDEB, and in lipid-loaded COS cells (42). Our date demonstrates that the generalized cellular machinery present in HeLa cells is sufficient for lipid droplet localization of CIDEs, without the need for additional cell type-specific proteins present in adipocytes in the case of CIDEA and FSP27 or in hepatocytes in the case of CIDEB.

We next assessed the degree of FSP27-mediated apoptosis of HeLa cells in the presence and absence of exogenous oleic acid supplementation. Figure 2*B* shows that 40% cell death was observed in FSP27 induced-apoptosis in HeLa cells when cultured in regular growth medium (i.e., no exogenous oleic acid). However, induction of lipid droplets in these cells via oleic acid supplementation of medium results in partially rescuing FSP27-mediated apoptosis such that only 20% cell death is observed. This suggests that physical localization of FSP27 at lipid droplets can inhibit its proapoptotic action. These data also indicate that the same region of FSP27 protein may be responsible for both apoptotic effect and lipid droplet localization. It is not currently known whether FSP27 might undergo regulated dissociation from lipid droplets; however, lipid droplets are highly dynamic organelles that possess multiple proteins associated with intracellular trafficking (10, 18, 38).

ATGL expression inhibits FSP27-induced lipid droplets. ATGL has recently been demonstrated to be the first and rate-limiting step in triacylglycerol hydrolysis. The sequential actions of ATGL, hormone-sensitive lipase, and monoglyceride lipase result in release of energy from stored lipid droplets as fatty acid and glycerol (43). In addition to its role in adipocyte hormone-sensitive triacylglycerol hydrolysis, ATGL has also been demonstrated to function in basal lipolysis (31). Ectopic expression of ATGL in oleic acid-cultured HeLa cells significantly diminished triacylglycerol stores and the size of lipid droplets, whereas knockdown of ATGL under these culture conditions resulted in enhanced triacylglycerol accumulation and the formation of markedly larger lipid droplets (31). Although the mechanism(s) used by FSP27 to enhance lipid droplet size and triacylglycerol storage has not yet been identified, observations to date support the general hypothesis of shielding the triacylglycerol in lipid droplets from hydrolysis by lipases rather than by stimulating lipogenesis.

We examined the effect of ATGL expression on FSP27-mediated lipid droplet accumulation in HeLa cells cultured in the presence of oleic acid, wherein cells were subjected to cotransfection for concomitant expression of ATGL and FSP27. Cells were cotransfected with a 1:5 ratio of expression constructs for FSP27 and ATGL or expression construct for FSP27 with empty pcDNA3.1 vector and were supplemented with 400 μM BSA-complexed oleic acid upon medium change at 4 h posttransfection. Cells were stained for neutral lipid content the next day. The photomicrographs in Fig. 3*A* show representative microscopic fields of these cultures stained with Bodipy 493/503 or LipidTox Red. Many of the cells cotransfected with FSP27 and pcDNA EV showed evidence of enlarged lipid droplets (Fig. 3*A*, *right*); however, those cotransfected with FSP27 and ATGL have a dramatic reduction in numbers of cells with enlarged lipid droplets (Fig. 3*A*, *left*). The 1:5 ratio was chosen to ensure that if cells were transfected with FSP27, they likely also harbored the expression construct for ATGL. We have found that by using the maximum mass of FSP27 DNA for transfection, the vast majority of cells form enlarged lipid droplets. However, the mass of FSP27 expression construct we could utilize for these transfections was constrained by the 1:5 ratio. As such, some cells in the population escaped FSP27 transfection, and therefore, they did not form enlarged lipid droplets, as evidenced in Fig. 3*A*, *right*. The data for the effect of cotransfection of ATGL on FSP27-induced lipid droplet enlargement is quantified in Fig. 3*B*, wherein the numbers of cells with large lipid droplets per microscopic field were enumerated. The percentage of cells with one or more large lipid droplets is reduced by 70% in the presence of ATGL cotransfection.

To more specifically address the effect of ATGL on formation of FSP27-induced lipid droplets, we generated an ATGL expression construct wherein transfected cells were trackable by eGFP signal. To eliminate concerns over alterations in ATGL action due to expression as a fusion protein, we chose not to use an ATGL-eGFP fusion for these studies. Rather, we expressed ATGL using the internal ribosome entry site vector pIRES2-eGFP from a construct we designate as pIRES2-eGFP-ATGL. Cotransfection studies were conducted using pIRES2-eGFP-ATGL and FSP27. Cells were cotransfected, medium was supplemented with 400 mM oleic acid at 4 h posttransfection, and cultures stained the next day for neutral lipid with LipidTox Deep Red. Because ATGL-expressing cells could be tracked by eGFP signal, this allowed us to use a 5:1 ratio of FSP27 vs. pIRES2-eGFP-ATGL. This enabled a higher degree of transfection efficiency in regard to FSP27, with a large majority of cells in the cultures cotransfected with FSP27 and pcDNA EV demonstrating lipid droplet formation. In Fig. 3*C*, FSP27 transfectants that harbor EV pIRES2-eGFP show enlarged lipid droplets in nearly all of the green cells (Fig. 3*C*, *bottom*). On the other hand none of the green cells in Fig. 3*C*, *top*, show evidence of enlarged lipid droplets, whereas their neighboring nongreen cells do. These results are quantified by cell counting in Fig. 3*D* and by flow cytometry analysis of transfected eGFP+ green cell populations for LipidTox Deep Red signal in Fig. 3*E*. Figure 3*D* indicates a 78% reduction in the number of green cells with enlarged lipid droplets. Flow cytometry analysis in Fig. 3*E* indicates a 60% reduction in the mean LipidTox Deep Red signal intensity for green cells harboring pIRES2-eGFP-ATGL vs. green cells harboring pIRES2-eGFP EV. Together, these data indicate that, under conditions where FSP27 and ATGL are simultaneously coexpressed by cotransfection, ATGL is highly effective at inhibiting FSP27-mediated lipid droplet content.

The above study utilized cotransfection of ATGL and FSP27. As such, it is possible that the inhibitory action observed for ATGL is due to its lipolysis-promoting effects on the tiny nascent lipid deposits/droplets that form in response to incubation with oleic acid, and whose formation is not dependent on FSP27 action. Because these nascent droplets may

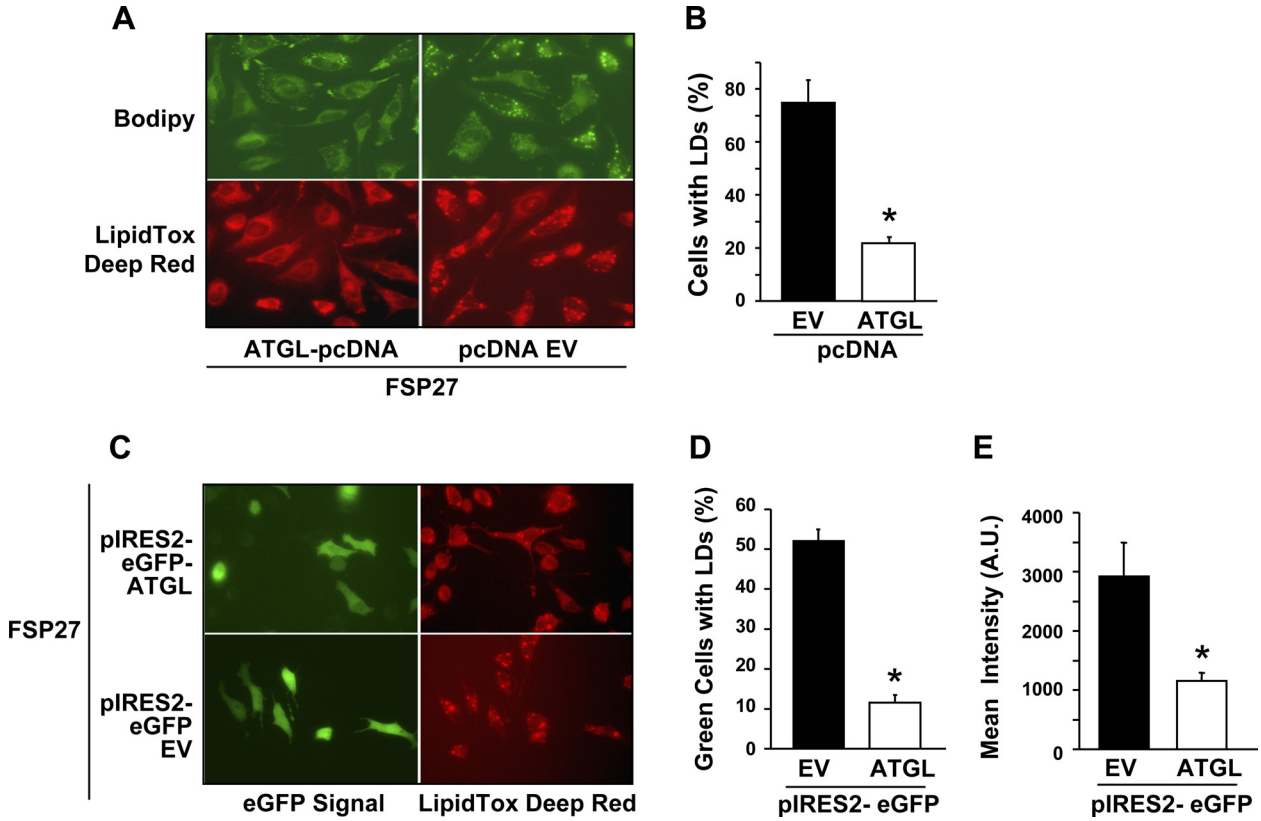

Fig. 3. Effect of cotransient expression of adipose triglyceride lipase (ATGL) on ability of FSP27 to promote lipid droplet formation. *A*: HeLa cells were transfected with an expression construct for FSP27 in the presence or absence of a 5-fold excess of an ATGL expression construct or an EV (pcDNA3.1). Cells were switched to culture medium supplemented with 400 μM BSA-complexed OA at 4 h posttransfection and at 12–14 h posttransfection were stained for lipid droplet content with Bodipy 493/503 (*top*) or LipidTox Deep Red (*bottom*) and photographed. Typical fields are depicted. *B*: the numbers of cells with 1 or more prominent enlarged lipid droplets (LDs) were enumerated per microscopic field, as described in MATERIALS AND METHODS. Data are shown as means ± SD. *C*: HeLa cells were transfected with a 5:1 ratio of FSP27 and either pIRES2-eGFP-ATGL or pIRES2-eGFP EV. Cells were switched to culture medium supplemented with 400 μM BSA-complexed OA at 4 h posttransfection and at 12–14 h posttransfection were stained for lipid droplet content with LipidTox Deep Red, imaged for eGFP and LipidTox Red signals, and photographed. Typical fields are depicted. *D*: the numbers of green cells with 1 or more prominent enlarged lipid droplets were enumerated per microscopic field for quadruplicate transfections, as described in MATERIALS AND METHODS. *E*: quadruplicate cultures of cells as depicted in *C* and *D* were subjected to flow cytometry analysis for eGFP and LipidTox Deep Red signals. Mean LipidTox Deep Red signal intensity per green cell is shown on *y*-axis. AU, arbitrary units. For *B*, *D*, and *E*, data are shown as means ± SD. $*P < 0.01$ vs. EV.

serve as a substrate for FSP27-mediated lipid droplet enlargement, it is possible that ATGL inhibits the ability of FSP27 to exert lipid droplet enlargement by diminishing the cellular content of these nascent droplets. To more fully explore the relationship between ATGL and FSP27 in regard to lipid droplet content, we next addressed the effect of ATGL on lipid droplets that were preformed via FSP27 action. To do so, we generated a stable cell population of FSP27-expressing HeLa cells using retroviral expression. Figure 4*A* compares lipid droplet content of these HeLa-FSP27 cells with that of EV control cells in the presence and absence of exogenous oleic acid. HeLa-FSP27 cells readily form small, clearly visible, and demarcated lipid droplets in the absence of exogenous oleic acid and show evidence of enlarged lipid droplets when cul-

Fig. 4. Effect of ATGL on preformed FSP27-induced lipid droplets. *A*: lipid droplet accumulation in HeLa cell populations stably expressing retrovirally driven FSP27 or pBABE-puro EV. *Left*: phase contrast pictures of EV and FSP27-expressing cells cultured for 1 day with (+OA) and without (−OA) 400 μM BSA-complexed OA; *right*: Bodipy 493/503 staining for lipid droplets. Phase contrast and Bodipy represent different cell fields with typical fields depicted. *B*: transient transfection of HeLa-FSP27 cells with ATGL or EV. Cells were incubated with 400 μM BSA-complexed OA for 24 h then transiently transfected with ATGL-pcDNA3.1 or EV. Cells were stained for lipid with Bodipy 493/503 at 12–14 h posttransfection with typical fields depicted. *C*: quantification of cells with lipid droplets that were transfected and cultured as in *B*. The numbers of cells with 1 or more prominent enlarged lipid droplets were enumerated per microscopic field in quadruplicate transfections, as described in MATERIALS AND METHODS. *D*: quantification of lipid droplet content per cell. Flow cytometry analysis for Bodipy 493/503 signal. Cells were transfected and cultured as for *B* and *C* in quadruplicate, with mean signal intensity per cell shown on *y*-axis. *E*: transient transfection of HeLa-FSP27 cells with pIRES2-eGFP-ATGL or pIRES2-eGFP EV. Cells were incubated with 400 μM BSA-complexed OA for 24 h then transiently transfected with pIRES2-eGFP-ATGL or pIRES2-eGFP EV. Cells were stained for lipid with LipidTox Deep Red at 12–14 h posttransfection. Typical fields are depicted. *F*: quantification of quadruplicate samples of cells with lipid droplets that were transfected and cultured as in *E*. %Green cells with 1 or more prominent enlarged lipid droplets was enumerated per microscopic field in quadruplicate, as described in MATERIALS AND METHODS. *G*: quantification of lipid droplet content per green cell. Cells were transfected and cultured as in *E* and *F*. Flow cytometry analysis was done on quadruplicate samples for eGFP and LipidTox Deep Red signal, with mean LipidTox Deep Red signal intensity per green cell shown on *y*-axis. *H–J*: experiments were carried out in quadruplicate as for *E–G*, except that cells were cultured with 400 μM BSA-complexed OA for 3 days prior to transfection. For *C*, *D*, *F*, *G*, *I*, and *J*, data are shown as means ± SD. $*P < 0.01$.

tured in oleic acid. Although the control EV cells show multiple punctuate areas of Bodipy lipid staining, as is usually observed for naive HeLa cells under oleic acid culture conditions, they do not form clearly evident lipid droplets. To test the effects of ATGL on preformed FSP27-mediated lipid droplets, HeLa-FSP27 cells were induced to form lipid droplets by culturing for 24 h in 400 μM BSA-complexed oleic acid followed by transfection with an expression construct for ATGL. Bodipy 493/503 staining in Fig. 4*B* shows the result of transient transfection with ATGL-pcDNA compared with cells transfected with pcDNA EV. Although nearly all cells in the EV show enlarged lipid droplet content, many cells in the ATGL-transfected population lack evident lipid droplets. This is enumerated in Fig. 4*C*, which shows a 25% reduction in cells with enlarged lipid droplets upon ATGL expression, and flow cytometry analysis for Bodipy signal in Fig. 4*D* shows a 28% reduction in mean signal intensity.

As was done in studies in Fig. 3, we also utilized pIRES2-eGFP-ATGL for these analyses. Figure 4*E* reveals that whereas all of the green cells in the pIRES2-eGFP-EV popu-

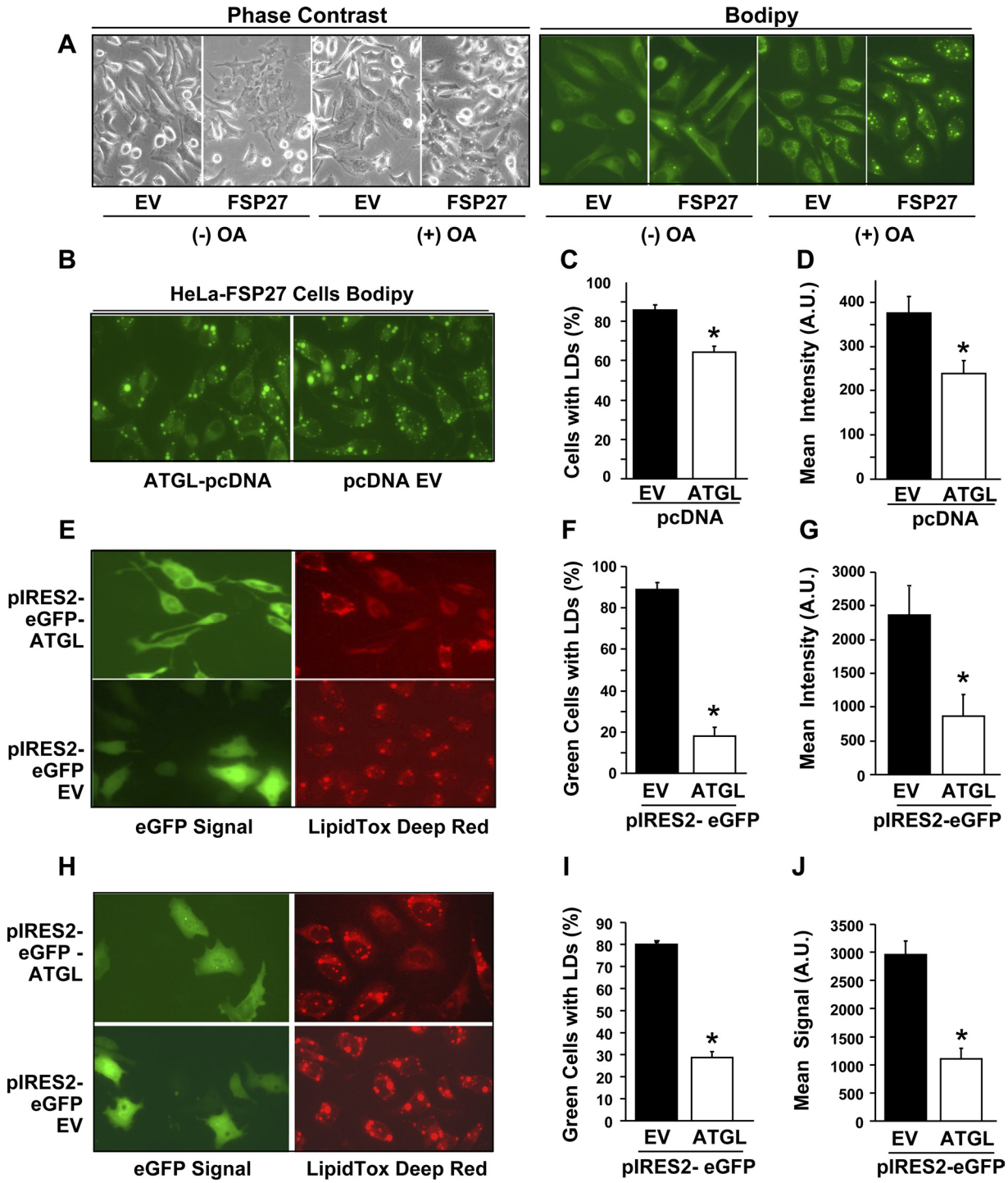

lation possess enlarged lipid droplets, as shown by LipidTox Deep Red staining, lipid droplet staining is dramatically reduced in the green cells harboring the pIRES2-eGFP-ATGL construct. Enumeration of green cells for lipid droplets in Fig. 4*F* and the corresponding flow cytometry data for LipidTox Deep Red signal in Fig. 4*G* reveal an 80 and 63% decrease, respectively, upon expression of ATGL. As shown in Fig. 4, *H–J*, we also conducted these studies using HeLa-FSP27 cells wherein FSP27-mediated lipid droplets had been preformed by a 3-day incubation in 400 μM BSA-complexed oleic acid and found effects largely similar to those of the 1-day oleic acid incubation. Thus, in our experimental cell culture model, whether tested by concomitant expression via cotransfection or in the context of lipid droplets preformed via FSP27-mediated action, FSP27 is not effective at protecting lipid droplets from the effects of ATGL.

Caspase-dependent apoptosis by FSP27. Given that lipid droplet accumulation within cells diminished the cell death effect of FSP27, we next set out to further define its apoptotic mechanism. Our previous report on the detection of PARP and α-fodrin cleavage upon ectopic expression of FSP27 in mammalian cells suggested the involvement of caspase activation in the proapoptotic effects of FSP27 (13); however, the caspase dependence of FSP27-mediated apoptosis and other details of its apoptotic mechanism has not yet been examined. We first investigated effects of the pan-caspase inhibitor Z-VAD-FMK on FSP27-mediated apoptosis using transient expression in 293T cells, with inhibitor added at time of transfection. Extent of apoptosis was determined by cell death assay, DNA fragmentation, and cleavage of PARP and α-fodrin. As shown in Fig. 5, *A–C*, Z-VAD-FMK effectively blocked the proapoptotic effects of FSP27. The level of cell death in the absence or presence of Z-VAD-FMK is 92 and 39%, respectively ($P < 0.01$). As shown in Fig. 5*B*, DNA fragmentation upon FSP27 transfection was completely inhibited by Z-VAD-FMK. In the Western blot in Fig. 5*C*, the disappearance of full-length p116 PARP, the appearance of the p89 caspase cleavage product of PARP, and the p150 caspase cleavage product of α-fodrin are blocked by Z-VAD-FMK treatment. To address involvement of specific caspases in FSP27-mediated apoptosis, the levels of cleaved caspase-9, -7, and -3 were examined by Western blot. Figure 5*D* reveals that, compared with the EV controls, in cells transfected with an FSP27 expression construct, the protein levels for these cleaved caspases are increased at each of the four posttransfection time points examined. To further validate the involvement of the caspase-9-mediated cell death pathways in FSP27-mediated apoptosis, we utilized a well-characterized dominant negative form of caspase-9, CS9DN. CS9DN contains a single point mutation of C287A at the site of processing of procaspase-9 to the active cleaved form and has previously been demonstrated to be highly effective in inhibiting activation of endogenous caspase-9 (32). Figure 5E, *left*, shows that transfection of FSP27 alone resulted in 53% cell death. Cotransfection of the CS9DN expression construct effectively rescued this effect; these cultures showed evidence of only 13% cell death. Cotransfection of CS9DN also diminished the appearance of p89 cleaved PARP (Fig. 5*E*, *right*).

To determine whether the caspase pathways activated by FSP27 during apoptosis involved mitochondria-mediated actions, we conducted immunocytochemistry analysis for localization of cytochrome *c* in FSP27-transfected cells. To correlate cytochrome *c* localization with FSP27 transfection on a cell-by-cell basis, we utilized an eGFP-FSP27 expression construct, allowing for visualization of FSP27 transfection with fluorescence microscopy. As a negative control, cells were transfected with empty eGFP vector. eGFP expression and cytochrome *c* immunostaining were assessed at 20 h posttrans-

Fig. 5. The FSP27 apoptotic mechanism involves caspase-9 and release of mitochondrial cytochrome *c*. *A*: the pan caspase inhibitor Z-VAD-FMK diminishes FSP27-mediated cell death. 293T cells were cotransfected with EV (closed bars) or a FSP27 expression construct (open bars) along with a marker LacZ+ expression construct, as described in MATERIALS AND METHODS, with 20 μM Z-VAD-FMK or DMSO vehicle added at time of transfection. Cells were stained for LacZ activity at 24 h posttransfection and LacZ+ blue cells counted. Data are shown as means ± SD. #$P < 0.001$ for untreated or DMSO-treated FSP27-transfected cells vs. their EV-transfected counterparts. The value for the leftmost column was set to 100%. *$P < 0.001$ for Z-VAD-FMK-treated FSP27-transfected cells vs. untreated or DMSO-treated FSP27-transfected cells. *B*: inhibition of FSP27-mediated fragmentation by Z-VAD-FMK. 293T cells were transfected with FSP27 expression construct or EV and incubated with 20 μM Z-VAD-FMK, DMSO vehicle, 20 μM of the negative control peptide VA-FMK, or no additions. Genomic DNA was prepared and analyzed for fragmentation using ethidium bromide staining. M, DNA marker, with numbers to the right indicating base pairs. *C*: inhibition of FSP27-mediated poly-ADP-ribose polymerase (PARP) and α-fodrin cleavage by Z-VAD-FMK. 293T cells were transfected with FSP27 expression construct and incubated with 20 μM Z-VAD-FMK, DMSO vehicle, 20 μM of the negative control peptide VA-FMK, or no additions. Cell lysates were harvested, and Western blot analysis was performed for full-length p116 and p89 cleaved PARP and p150 cleaved α-fodrin. NT, nontransfected. *D*: Western blot assessment of cleaved caspases. 293T cells were transfected with FSP27 expression construct or EV, and total protein was prepared at the indicated time points posttransfection. Western blot analysis was performed for p37 cleaved caspase-9 (CS9), p20 cleaved caspase-7 (CS7), and p19 cleaved caspase-3 (CS3). *E*: effects of expression of dominant negative caspase-9 (CS9DN) on FSP27-mediated apoptosis. *Top*: 293T cells were cotransfected with a LacZ expression construct and as either EV or expression constructs for FSP27 and/or CS9DN in the indicated combinations. Values of 1 and 7 represent 0.5 and 3.5 μg of the FSP27 and the CS9DN expression constructs, respectively. Cells were stained for β-galactosidase activity at 48 h posttransfection and blue (LacZ+) cells counted. Data are shown as means ± SD. *$P < 0.001$ for FSP27-transfected cells compared with EV-transfected cells; #$P < 0.001$ for FSP27 and CS9DN cotransfected cells compared with FSP27-transfected cells. The value of the leftmost samples was set to 100%. *Bottom*: 293T cells were cotransfected as described directly above for cell death assay and analyzed by Western blot using anti-caspase-9 and anti p89 cleaved PARP antibodies. The mass of the FSP27 and CS9DN expression construct used in micrograms are indicated at *top*. For *B–E*, images shown in the same agarose gel or in the boxed horizontal Western blots were run on the same gel and, in case of Western blots, processed on the same membrane. However, in some instances lanes have been removed and/or rearranged for economy and clarity of presentation. *F*: assessment of cytochrome *c* release. COS cells were transiently transfected with an expression construct for eGFP-FSP27 or eGFP EV. Shown are eGFP signal under FITC fluorescence (green; *top*) and cytochrome *c* (Cyto *c*) immunostaining using a monoclonal cytochrome *c* primary antibody with Alexa fluor 568-conjugated secondary antibody (red; *middle*). Nuclei stained with 4,6-diamidino-2-phenylindole (DAPI) are shown at *bottom*. The meaning of the arrows and asterisks is described in the text. Representative images are shown. *G*: Western blot analysis for quantification of Cyto *c* release to cytoplasm. COS cells were transiently transfected with eGFP-FSP27 (full) or EV and analyzed at 18 h posttransfection. *Top*: 6 μg of cytosolic fraction protein analyzed by Western blot for Cyto *c*, the cytosolic marker protein GAPDH, and the mitochondrial marker ATP synthase; this blot also contained 10 μg of purified mitochondria fraction protein, with short (S) and long (L) exposures shown. Samples were prepared independently from triplicate transfections. Data shown within each boxed area arose from the same protein gel. *Bottom*: digital quantification of Western blot signals. Data are shown as means ± SD. *$P < 0.01$ vs. EV.

fection. Figure 5*F* reveals that cells expressing eGFP-FSP27, and therefore green in appearance, show a diffuse cytoplasmic distribution of red signal for immunostained cytochrome *c*, indicative of release of cytochrome *c* from mitochondria. These cells are designated by arrows in Fig. 5*F*, *middle left*. A nontransfected cell present in this same field is depicted by an asterisk and shows cytochrome *c* staining only in the distinctive spaghetti-like pattern that is typical of intact mitochondria. All three images in Fig. 5*F*, *right*, show an EV eGFP transfected and a nontransfected cell, indicated by asterisks, in which the typical mitochondrial localization pattern for cytochrome *c* is observed. We quantified the release of cytochrome *c* to the cytosol by Western blot analysis (Fig. 5*G*). COS cells were transfected with eGFP-FSP27 or eGFP EV and cytosolic fractions prepared and analyzed by Western blot for cytochrome *c* as well as for the cytosolic marker GAPDH and the mitochondrial marker ATP synthase-α. The Western blot data in the Fig. 5*G*, *top*, reveal a dramatic increase of cytosolic cytochrome *c* level in cells transfected with eGFP-FSP27 vs. EV. The GAPDH and ATP synthase data panels reveal that this

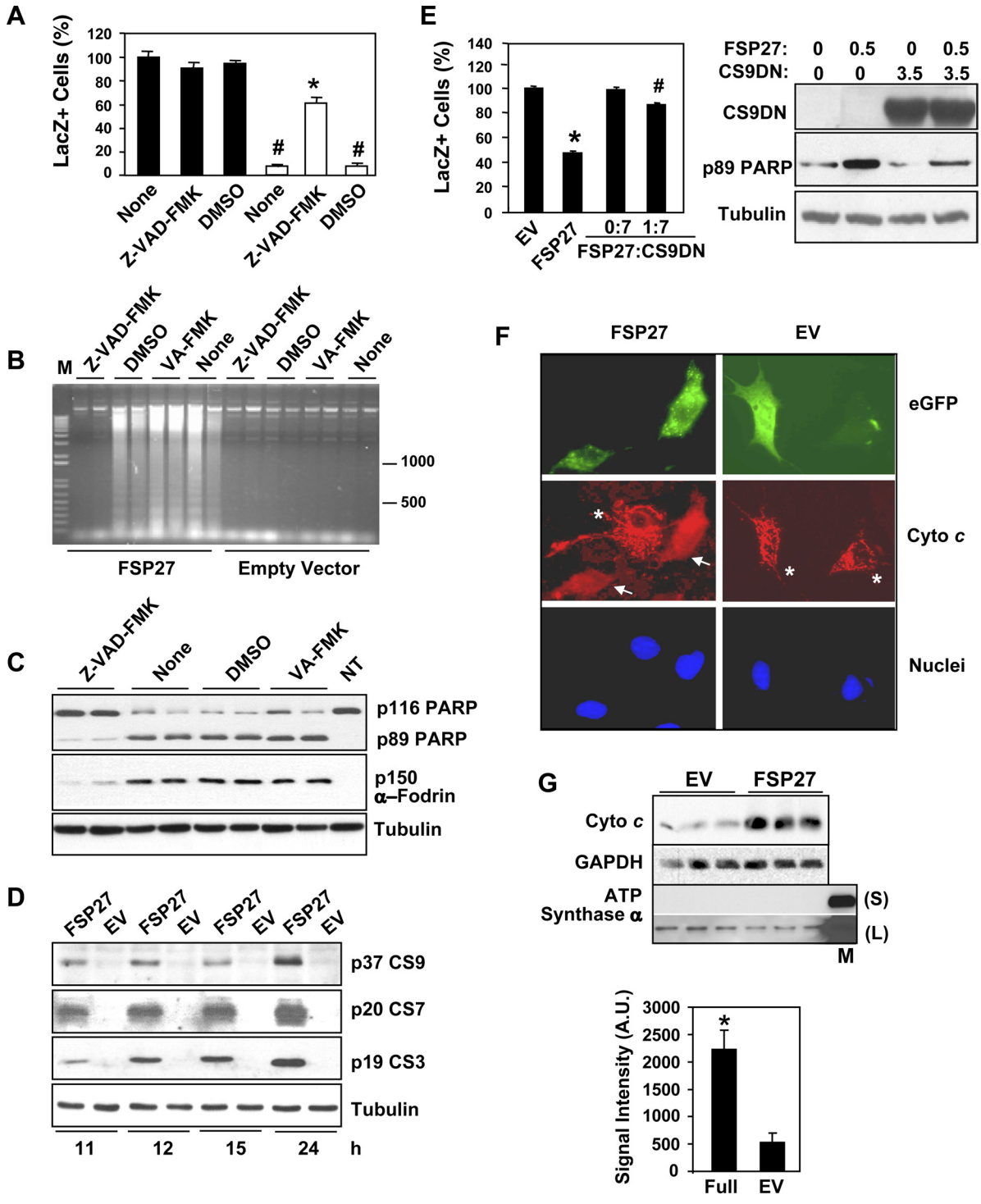

is due to the effects of eGFP-FSP27 rather than protein loading differences or any differential mitochondrial contamination of samples. The cytochrome *c* signal is quantified in the graph in Fig. 5*G*, *bottom*.

Overall, our studies indicate that a caspase-dependent mitochondrial-mediated mechanism is involved in FSP27-induced cell death. The role of caspases in the apoptotic mechanism of CIDEA and CIDEB remains to be fully explored. In the initial cloning report for CIDEA and CIDEB, it was indicated that apoptosis induced by transient expression of CIDEA in 293T cells was caspase independent due to the failure of caspase inhibitor, when added at 8 h posttransfection, to block CIDEA-mediated apoptosis (11). On the other hand, a study of CIDEB supported a caspase-dependent mechanism of action in that activity of caspase-3, and release of mitochondrial cytochrome *c* occurred upon transient expression of CIDEB in COS cells (8). It remains to be determined whether the apoptotic mechanism of CIDEA differs from that for FSP27 and CIDEB or whether the early report of caspase independence for CIDEA might be due to the rather late timing of addition of caspase inhibitor in that study (11).

The same subregion of the FSP27 CIDE C domain governs apoptotic activity and lipid droplet localization. We next addressed the region(s) of FSP27 responsible for apoptotic function and for lipid droplet localization, initially using eGFP fusions for full-length FSP27 or containing the CIDE N domain (FSP27-N) or the CIDE C domain (FSP27-C) of FSP27 fused COOH terminal to eGFP. Figure 6*A* reveals that 70% cell death is observed for full-length FSP27 and 65% cell death is observed for FSP27-C. In contrast, FSP27-N shows evidence of 18% cell death. Thus the vast majority of the apoptotic effect of FSP27 is attributable to actions of its CIDE C domain. In contrast to FSP27-N, expression of FSP27-C leads to the appearance of marked DNA fragmentation (Fig. 6*B*) and generation of the cleaved proteins for PARP, α-fodrin, and active cleaved forms of caspase-9, -7, and -3 (Fig. 6*C*). Figure, 6, *D* and *E*, confirms that FSP27-C-mediated apoptosis, as we have shown herein for full-length FSP27, is caspase dependent in that it is effectively inhibited by Z-VAD-FMK. This is both in regard to cleaved PARP and α-fodrin levels (Fig. 6*D*) and DNA fragmentation (Fig. 6*E*). Although a slight increase in cell death effect was also found for FSP27-N in the assay used in Fig. 6*A*, no evidence of FSP27-N-mediated apoptosis was noted in regard to DNA fragmentation or by Western blot analysis of apoptotic markers (Fig. 6, *B* and *C*). We also observed, as we found for full-length FSP27, that expression of FSP27-C promoted release of mitochondrial cytochrome *c* (Fig. 6*F*), but expression of FSP27-N did not. As was done for Fig. 5*G*, we compared and quantified cytochrome *c* release for FSP27-N and FSP27-C by Western blot (Fig. 6*G*). Although a significant increase in cytosolic cytochrome *c* was found for FSP27-C vs. empty eGFP vector, this was not observed for FSP27-N.

We next used confocal microscopy to examine the ability of the FSP27-N or FSP27-C to localize to lipid droplets. eGFP-FSP27, eGFP-FSP27-N, or eGFP-FSP27-C was transfected into HeLa cells that had been precultured in the presence of exogenous oleic acid to stimulate lipid droplet accumulation. Figure 6*H* clearly shows that signal for eGFP-FSP27-N is distributed throughout the cytoplasm with no particular signal enrichment at lipid droplets. In contrast, eGFP-FSP27-C shows distinct and clear localization with green signal that is localized specifically in a ring around the Nile red-stained lipid droplets.

To better map the region of FSP27 governing its apoptotic activity and lipid droplet localization, two NH_2-terminal deletion constructs of eGFP-FSP27-C were generated, eGFP-FSP27-Δ173 and eGFP-FSP27-Δ192 (Fig. 7*A*, *top*). These were tested for apoptotic activity and lipid droplet localization. Figure 7*A*, *bottom*, indicates that FSP27-Δ173 has robust cell death activity. In contrast, eGFP-FSP27-Δ192 had no discernable effects on cell viability. eGFP-FSP27-Δ173 is capable of inducing DNA fragmentation (Fig. 7*B*) and the generation of cleaved p89 PARP and active caspase-9,-7, and -3, as shown by the Western blot in Fig. 7*C*. This is in marked contrast to eGFP-FSP27-Δ192, which has only minor effects on chromosomal DNA integrity and no evident generation of apoptotic markers by Western blot. Apoptosis mediated by eGFP-FSP27-Δ173 is caspase-dependent, as the addition of Z-VAD-FMK abrogates the appearance of p89 PARP and activated caspases, as shown by Western blot in Fig. 7*D*. These results suggest that the 19-amino acid region from 173 to 192 is critical for the major apoptotic activity of FSP27 and that the mechanism of apoptosis that maps to this region appears to be the same as that for full-length FSP27 in that both are caspase dependent.

We next assessed whether the ability of the FSP27 deletions to induce caspase-dependent apoptosis tracked with their lipid droplet localization, as we had demonstrated in Fig. 6 with respect to FSP27-C. Figure 7*E* shows confocal localization of eGFP-FSP27-Δ173 and eGFP-FSP27-Δ192 assessed in transfected HeLa cells cultured in the presence of exogenous oleic acid, with lipid droplets stained with Nile red. eGFP-FSP27-Δ173 shows clear localization to lipid droplets. In contrast, eGFP-FSP27-Δ192 shows a uniform distribution of eGFP signal throughout the cytoplasm, as we noted previously for eGFP EV and for eGFP-FSP27-N. To obtain additional information on the amino acid sequences that may function as a discrete signal for FSP27 localization to lipid droplets, we generated a small peptide that was fused COOH terminal to eGFP that contained the 19 amino acids spanning from amino acids 173 to 192 of the FSP27 CIDE C domain, termed eGFP-FSP27-19AA. Analysis of HeLa cells cultured with exogenous oleic acid and transfected with eGFP-FSP27-19AA shows that signal for this fusion protein fails to localize to lipid droplets, appearing instead to be distributed evenly throughout the cytoplasm, similar to what was found for eGFP-FSP27-Δ192. eGFP-FSP27-19AA also failed to show evidence of cell death, inducing activity (data not shown). Thus, our data indicate that amino acids 173–192 of the FSP27 CIDE C domain are necessary for both robust apoptosis and for localization to lipid droplets but that this region alone is not sufficient for either effect. Our findings on the role of the CIDE C domain of FSP27 are in line with that reported by Keller et al. (12), who observed that full-length FSP27 and an expression construct containing its CIDE C domain promote apoptotic morphology of 293T cells. These workers also showed that 3T3-L1 adipocytes expressing full-length FSP27 or the CIDE C expression construct showed enhanced sensitivity to TNFα-mediated apoptosis, as assessed by terminal deoxynucleotidyl-mediated dUTP nick-end labelingstaining (12). However, no further indexes or markers of apoptotic activity were assessed, nor was further mapping of these functions or those

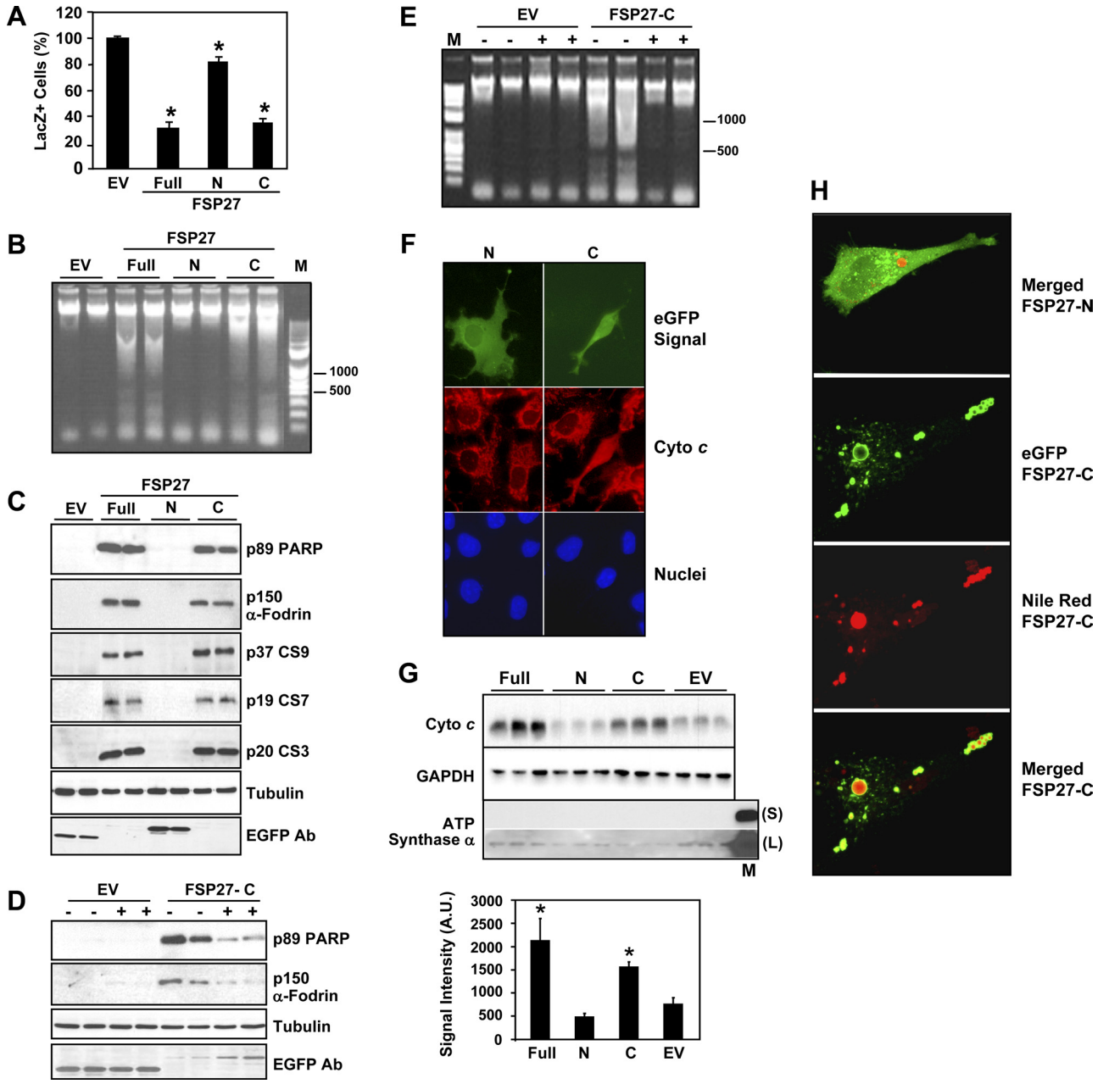

Fig. 6. FSP27-C is necessary and sufficient for caspase-mediated apoptosis and lipid droplet localization. *A*: cell death assay. 293T cells were cotransfected with EV, full-length FSP27 (full), FSP27-N, or FSP27-C as eGFP fusion constructs together with a LacZ expression construct. Cells were stained for β-galactosidase (LacZ+) and blue cells counted at 48 h posttransfection. Data are shown as mean ± SD. *$P < 0.001$ compared with EV-transfected cells. Levels in the EV sample were set to 100%. *B*: DNA fragmentation assay. 293T cells were transfected with EV or the indicated eGFP FSP27 fusion constructs (N, FSP27-N; C, FSP27-C). Genomic DNA was prepared at 48 h posttransfection and analyzed by SYBR green staining. *C*: Western blot assessment of apoptotic indexes. Total protein was harvested from 293T cells at 48 h posttransfection and Western blot analysis performed for indicated proteins. *D*: inhibition of cleavage of PARP and α-fodrin by Z-VAD-FMK. 293T cells were transfected with EV or eGFP-CIDE C expression construct and cultured in the absence (−) or presence (+) of Z-VAD-FMK for 24 h. Total protein was harvested and analyzed by Western blot for PARP or α-fodrin. *E*: inhibition of DNA fragmentation by Z-VAD-FMK. 293T cells were transfected with eGFP EV or eGFP-CIDE C expression construct and cultured in the absence (−) or presence (+) of Z-VAD-FMK for 24 h. Genomic DNA was harvested and assessed by SYBR green staining. Due to the degree of cell death-mediated FSP27 and FSP-C, the respective eGFP fusion proteins are not visible in the exposures shown in Western blot of these cell lysates. For *B–E*, images shown in the same agarose gel or in the boxed horizontal Western blots were run on the same gel and, in case of Western blots, processed on the same membrane. However, in some instances lanes have been removed and/or rearranged for economy and clarity of presentation. *F*: FSP27-C mediates release of mitochondrial Cyto *c* to cytoplasm. COS cells were transiently transfected with N or C. Shown are eGFP signal under FITC fluorescence (green; *top*), Cyto *c* immunostaining using a monoclonal Cyto *c* primary antibody with Alexa fluor 568-conjugated secondary antibody (red; *middle*), and nuclei stained with DAPI (blue; *bottom*). Representative images are shown. *G*: Western blot analysis for quantification of Cyto *c* release by eGFP-FSP27-CIDE C. COS cells were transiently transfected with eGFP-FSP27 (full), N, C, or eGFP EV and analyzed at 18 h posttransfection. *Top*: 6 μg of cytoplasmic fraction protein analyzed by Western blot for Cyto *c*, the cytoplasmic marker protein GAPDH, and the mitochondrial marker ATP synthase-α; the ATP synthase-α blot also contained 10 μg of purified mitochondria fraction protein with S and L exposures shown. Samples were prepared independently from triplicate transfections. Data shown within each boxed area arose from the same protein gel. *Bottom*: digital quantification of Western blot signals. Data are shown as means ± SD. *$P < 0.01$ vs. EV. *H*: localization of FSP27-N and FSP27-C in lipid-loaded HeLa cells. Cell culture, transfection, and analysis were carried out as described for Fig. 2*A*.

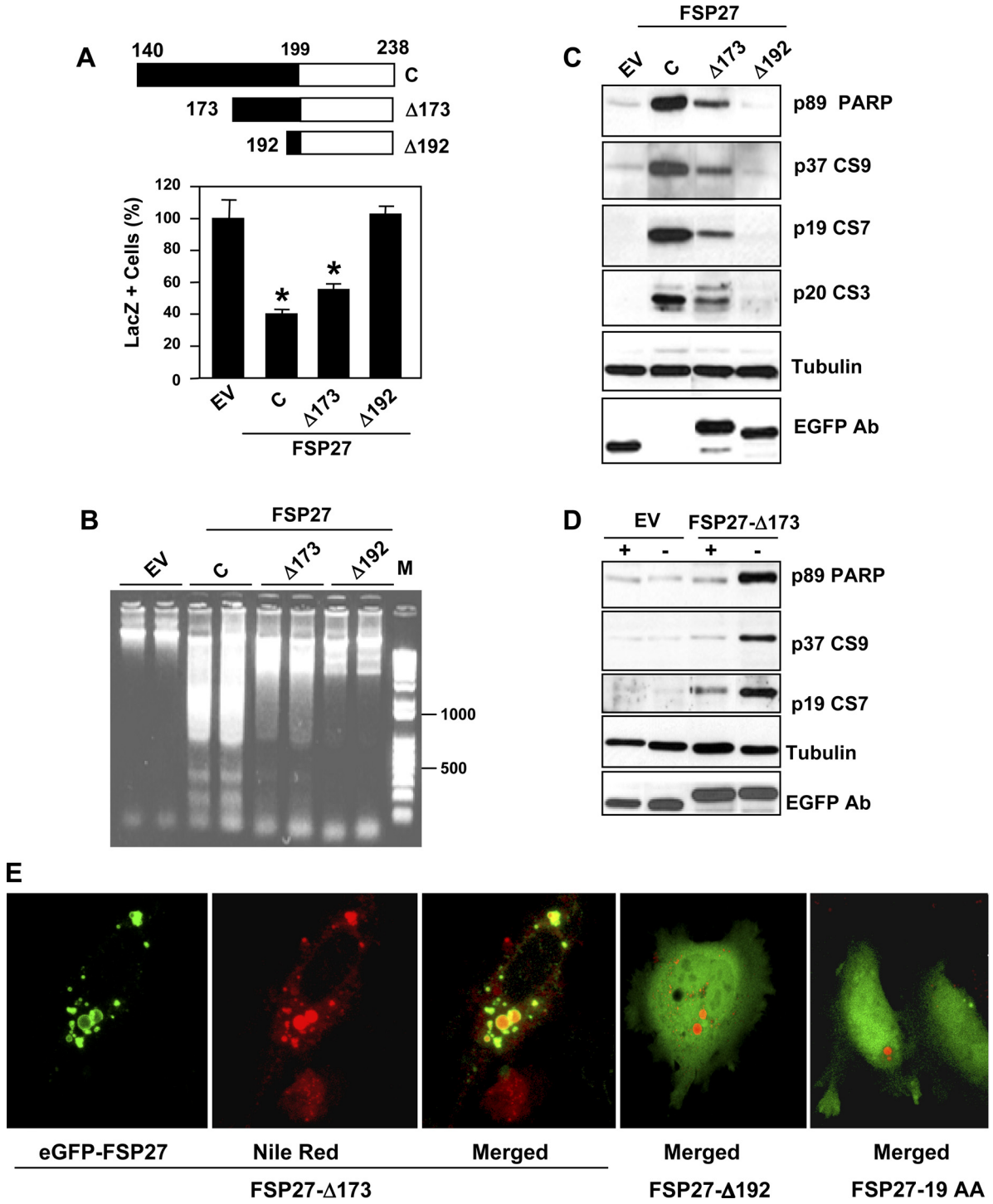

Fig. 7. Deletion analysis of the apoptotic and lipid droplet localization function of FSP27-C. *A*: effects of regions of the FSP27-C on apoptosis. *Top*: schematic representation of the eGFP-FSP27-C and deletion constructs. The CIDE C domain or regions thereof are represented in black, and numbers indicate amino acid positions in the FSP27 protein sequence. Constructs contain eGFP fusion 5′ to the indicated FSP27 coding regions. *Bottom*: 293T cells were cotransfected with EV, C, Δ173, and Δ192 expression constructs together with a LacZ expression construct, as described in MATERIALS AND METHODS. Cells were stained for β-galactosidase activity and blue cells (LacZ+) counted at 48 h posttransfection. Value for the EV was set to 100%. Data are shown as means ± SD. *$P < 0.001$ compared with EV-transfected cells. *B*: DNA fragmentation assay. 293T cells were transfected EV or the indicated eGFP-FSP27 fusion constructs. Genomic DNA was prepared at 24 h posttransfection and analyzed by SYBR green staining. *C*: Western blot assessment of apoptotic indexes for FSP27 deletions. Total protein was harvested at 48 h posttransfection and Western blot analysis performed for p89 cleaved PARP, CS9, CS7, CS3. *D*: effect of the pan caspase inhibitor Z-VAD-FMK on Δ173-mediated apoptosis. 293T cells were transfected with EV or the Δ173 expression construct and cultured in the presence (+) or absence (−) of Z-VAD-FMK for 24 h. Total protein was harvested and analyzed by Western blot for p89 cleaved PARP, CS9, and CS7. For *B–D*, images shown in the same agarose gel or in the boxed horizontal Western blots were run on the same gel and, in the case of Western blots, processed on the same membrane. However, in some instances lanes have been removed and/or rearranged for economy and clarity of presentation. *E*: lipid droplet localization of FSP27 deletion constructs. Cell culture, transfection, and analysis were carried out as described for Fig. 2*A*.

for regions of FSP27 governing lipid droplet targeting examined further. A recent report by Rubio-Cabezas et al. (30a) has described partial lipodystrophy and insulin-resistant diabetes in a patient with a homozygous nonsense mutation in FSP27/CIDEC at position 186. This mutation truncates and disrupts the CIDE C domain, further underscoring the role of this region in FSP27 function in WAT. It is of interest to note that this mutation occurs within that 19-amino acid stretch from 173 to 192 of the FSP27 CIDE C domain that we show herein is required for FSP27 localization to lipid droplets.

During the preparation of this article, a study on the localization of CIDEB to lipid droplets was reported (42). This revealed that the region of CIDEB from 166 to 195 directed localization of an eGFP-CIDEB fusion to lipid droplets in hepatocytes (42). In regard to protein sequence homologies between the three CIDE proteins, although they share homology within their respective CIDE C domains, the regions COOH terminal to their CIDE C domains are unique to each respective CIDE protein. We postulate that the region of the FSP27 CIDE C domain from amino acids 173 to 199 is involved in its lipid droplet localization; it is also likely that the homologous region governs lipid droplet localization for CIDEA.

Assessment of protein interaction for FSP27 and CIDEA. Studies to date indicate that protein-protein interactions are important to CIDE protein function, and both CIDEA and CIDEB have been studied somewhat in this regard. Homo- and heterodimeric interaction of CIDEA and/or CIDEB (i.e., CIDEA:CIDEA, CIDEB:CIDEB, and CIDEA:CIDEB) has been reported (5, 8, 11, 19, 27). CIDEB interacts with viral protein NS2 (8) and apolipoprotein B (42) and CIDEA with AMPK (27); such interactions appear to impact the physiological function of these CIDE partner proteins. In cases where protein regions for CIDEA- and CIDEB-mediated interactions have been mapped, they involve the respective CIDE C region (5, 8, 11, 27, 42). CIDEA and CIDEB were initially cloned on the basis sequence homology to the CIDE N domain of DFF45, the inhibitory regulatory subunit of the major apoptotic nuclease DFF40. To our knowledge, direct interactions mediated by CIDE N domains have been detected only in respect to interaction of CIDEB with the CIDE N domains of DFF40 and DFF45 and between the respective CIDE N domains for DFF40 and DFF45 (19). The physiological endogenous role of CIDEB-mediated apoptosis and its CIDE N domain-mediated

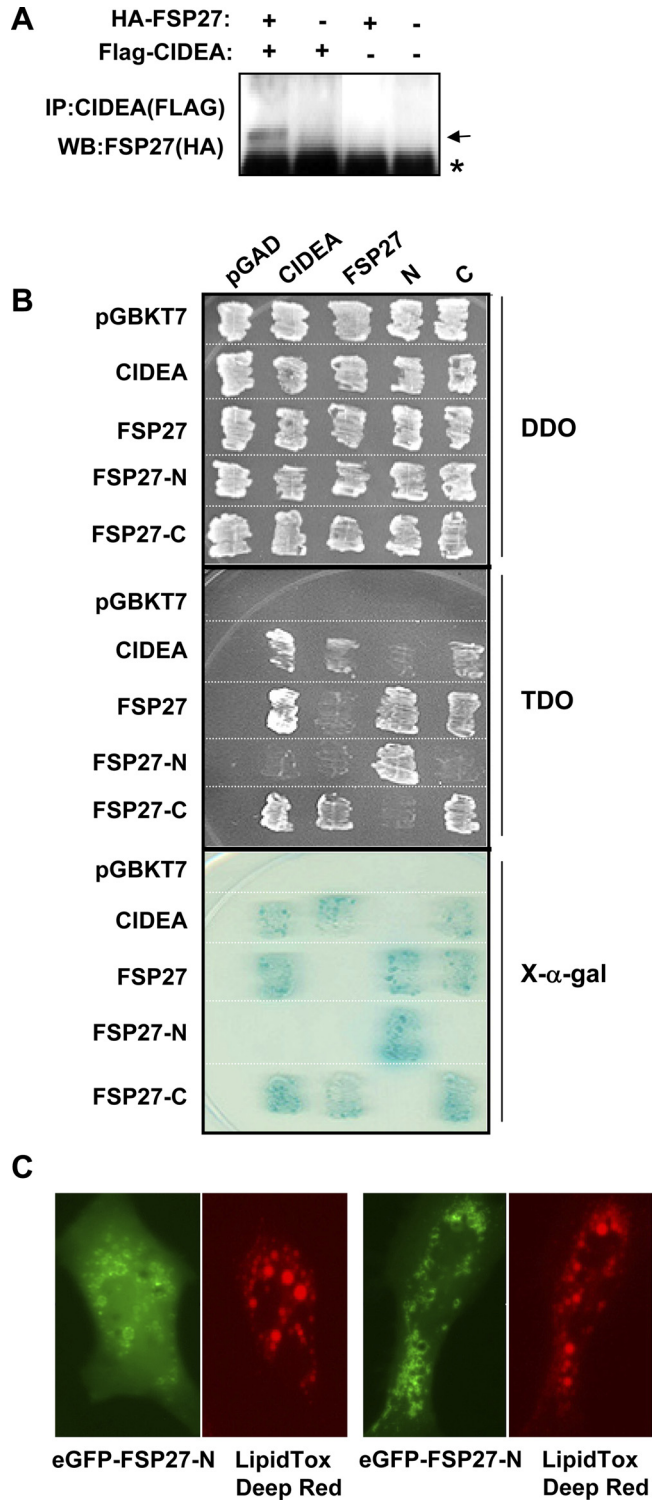

Fig. 8. Protein-protein interaction analysis of FSP27. *A*: coimmunoprecipitation analysis. 293T cells were cotransfected with HA-tagged FSP27 (HA-FSP27) (+), FLAG-tagged CIDEA (+), or EV (−). Total protein was harvested 48 h posttransfection, and cell lysates were immunoprecipitated with anti-FLAG M2-agarose followed by Western blotting with anti-HA antibody. A 10-s exposure is shown. ←HA signal; *nonspecific signal from antibody light chain. Images shown in the same boxed horizontal Western blots (WB) were run on the same gel and processed on the same membrane. However, in some instances lanes have been removed and/or rearranged for economy and clarity of presentation. *B*: Yeast two hybrid interaction assay. Yeast harboring the indicated combinations of the pGBTK7-based or pGAD-based yeast two hybrid expression constructs, listed at *top* and *left*, were inoculated onto on selective media. DDO, Leu and Trp double-dropout medium; TDO, His, Leu, and Trp triple-dropout medium; X-α-gal, TDO medium containing X-α-gal. Macroscopic view of yeast media plates is shown. *Middle* and *bottom* show growth and color indicative of protein-protein interaction. A thin dotted line has been added to aid in distinguishing each row. Images shown in each boxed area arose from the same agar plate. However, in some instances lanes have been removed and/or rearranged for economy and clarity of presentation. *C*: FSP27 can mediate lipid droplet localization of the FSP27 CIDE N domain. HeLa cells were incubated for 2 days with 400 μM BSA-complexed OA to induce lipid droplet formation and then transiently cotransfected with expression constructs for nontagged FSP27 and eGFP-FSP27-CIDE N. At ~16 h posttransfection, cells were stained for lipid with LipidTox Deep Red and observed by fluorescence microscopy and photographed. The *left* and *right* sets depict 2 examples typical for cells showing eGFP-FSP27-CIDE N signal at lipid droplets. Within each set, the *left* image shows eGFP signal for eGSP-FSP27-N and the *right* image lipid droplets stained with LipidTox Deep Red.

interactions remain undetermined. No information exists regarding protein-protein interactions for FSP27. Since FSP27 and CIDEA are both present at lipid droplets of human white adipocytes (25, 26), this raised the possibility of interaction of CIDEA and FSP27. To investigate this, we carried out cotransfection studies in 293T cells and assessed for FSP27-CIDEA interaction using coimmunoprecipitation. Figure 8*A*, *top*, reveals interaction of full-length FSP27 with full-length CIDEA.

Yeast two hybrid had previously been successfully employed and validated for assessment of CIDEB protein-protein interactions with regard to homodimerization and CIDEB heterodimerization with CIDEA, AMPK, and NS2 (8, 42). Technical issues with Western blots showing heavy signal arising from the immunoglobulin light chain precluded our further assessments by coimmunoprecipitation. Therefore, we utilized the yeast two hybrid protein-protein interaction method. For our analyses, full-length FSP27, FSP27-N, FSP27-C, and full-length CIDEA were expressed as Gal4 DNA binding domain and Gal4 DNA activation domain fusion proteins in yeast. Various pairwise combinations of the pGBKT7 binding domain and the pGAD activation domain-based expression constructs were transformed into AH109 strain *S. cerevisiae.* Effective cotransformation is illustrated by robust growth of yeast on DDO media lacking Trp and Leu (Fig. 8*B*, *top*). The interaction of the indicated pairs of expressed proteins is assessed in Fig. 8*B*, *middle* and *bottom*. Protein-protein interaction was scored by growth on TDO media lacking Trp, Leu, and His and the ability to cleave the chromogenic substrate X-α-gal to produce blue-colored growth. Here, we find the anticipated homodimeric interaction for CIDEA, which has been reported previously (27, 44). Figure 8*B* also shows that although full-length FSP27 does not show evidence of homodimerization, homodimerization is observed with the individual FSP27-N and FSP27-C constructs. We also find, as we had using coimmunoprecipitation, heterodimerization for CIDEA and full-length FSP27 and further demonstrate that FSP27-C functions in this interaction. FSP27-C interacts with full-length CIDEA and full-length FSP27 when FSP27-C is expressed as

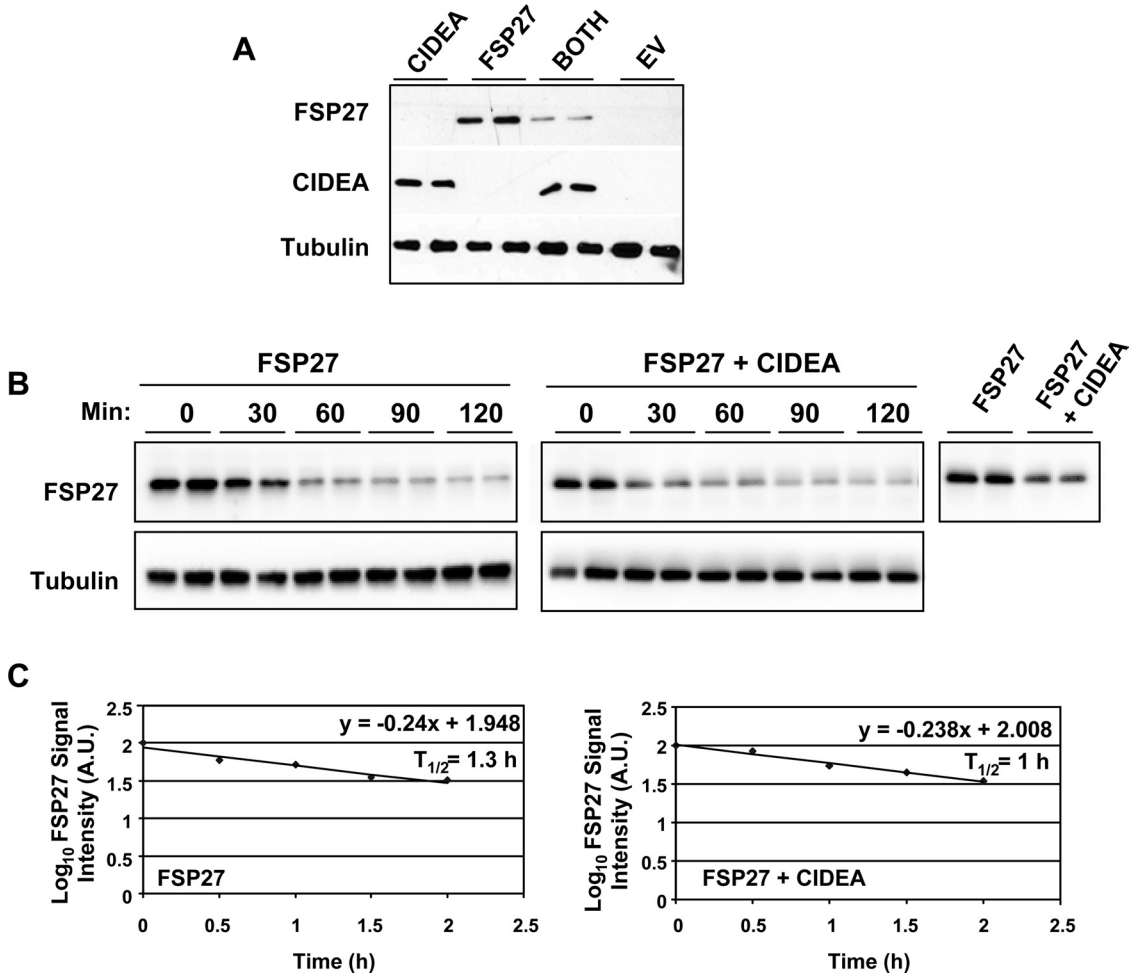

Fig. 9. Effect of CIDEA on FSP27 Protein Levels. *A*: Western blot analysis. 293T cells were transfected with expression constructs for HA-tagged FSP27 (FSP27), FLAG-tagged CIDEA (CIDEA), both, or EV. Total protein was harvested 48 h posttransfection, and cell lysates were assessed by Western blot using anti-FLAG and anti-HA antibodies. *B*: assessment of FSP27 protein stability. 293T cells were transfected with expression constructs for HA-tagged FSP27 (FSP27) in the absence and presence of cotransfection of FLAG-tagged CIDEA. Cells were treated with 100 μg/ml cycloheximide at 40 h posttransfection, with the 0 time point harvested just prior to cycloheximide treatment. Total protein was harvested at the indicated time points post-cycloheximide treatment, shown in min. Western blots were probed with indicated antibodies. For *A* and *B*, images shown in the same boxed horizontal Western blots were run on the same gel and processed on the same membrane. However, in some instances lanes have been removed and/or rearranged for economy and clarity of presentation. C: half-life determination. Graphical representation of quantitated signals from Western blot analyses is shown.

either a binding domain or activation domain fusion. In the intracellular milieu of the lipid droplet, it is possible that the proapoptotic CIDE C region of FSP27 is kept in check via interaction with other lipid droplet proteins, perhaps including CIDEA.

Although the FSP27-N domain interacts with full-length FSP27 when it is expressed as an activation domain fusion in pGAD, there is no evidence of this when FSP27-N is expressed as a binding domain fusion in pGBTK7. We have determined that full-length FSP27 localizes to lipid droplets, as does FSP27-C domain, whereas FSP27-N domain does not. These observations and our yeast two hybrid data suggested that, by interaction with full-length FSP27, the FSP27-N domain might show lipid droplet localization. To test this, we transiently cotransfected lipid-loaded HeLa cells with eGFP-FSP27-N and nontagged full-length FSP27. As shown in Fig. 8*C*, we observed multiple cells that showed a degree of eGFP signal at a subset of lipid droplets, suggesting lipid droplet localization of eGFP-CIDE N via interaction with full-length FSP27. However, we note that this was observed in only 1–3% of green cells. The vast majority of green cells demonstrated diffuse cytoplasmic signal, as shown in Fig. 6*H*. On the other hand, no evidence of lipid droplet localization of eGFP-FSP27-N was observed when cells were cotransfected with CIDEA in place of FSP27 cotransfection (data not shown). This is in line with our yeast two hybrid data showing no evidence of interaction for CIDEA with FSP27-N domain.

Interestingly, we had reported previously that both ectopically expressed FSP27 and FSP27 protein present in fat cells exist as multiple distinct species of size(s) consistent with that predicted to result from NH_2-terminal truncations (13). A major shorter FSP27 protein species of ~14 kDa that is consistent with the predicted mass of FSP27-C is present at readily detectable levels in 3T3-L1 adipocytes and FSP27-transfected COS cells (13). It is possible that in vivo not only does FPS27 exist as a full-length form but also as a processed/cleaved form that may generate FSP27 protein species containing CIDE N or CIDE C regions. On the basis of our data herein, these species of FSP27 protein would be predicted to demonstrate distinct activities with regard to apoptosis, lipid droplet localization, and protein-protein interaction. Our demonstration that the same region of FSP27 required for specific subcellular localization at the lipid droplet coincides with that required for its apoptotic activity suggests that the localization of FSP27 in the unique molecular niche of the lipid droplet may concomitantly mask the subregion of FSP27 that is necessary for its apoptotic activity. By extension, disrupting these interactions, some of which may be mediated by amino acids 172–192 of FSP27, may derail its lipid droplet association, possibly allowing FSP27 to exert other actions.

Studies in several mammalian cell lines of the stability of ectopically expressed CIDEA protein have shown that it undergoes rapid proteasomal degradation with a half-life of <30 min (4). Moreover, the recently identified CIDEA interaction partner AMPK undergoes greatly enhanced proteasomal degradation as a result of its interaction with CIDEA (27). The rapid proteasomal degradation of CIDEA is governed largely by ubiquitination of a lysine at amino acid position 23 of the CIDEA protein (4). This is NH_2 terminal to the CIDE N domain and as such outside of the region of shared CIDE N domain homology for CIDEA, CIDEB, and FSP27. A lysine does not appear conserved in this position or region of either CIDEB or FSP27, although other lysines are present. As we demonstrated interaction of CIDEA with FSP27, we investigated whether CIDEA might affect FSP27 protein stability. We first transfected 293T cells with CIDEA only, FSP27 only, or both constructs and assessed levels of respective protein expression at 48 h posttransfection. As is shown in the Western blot in Fig. 9*A*, coexpression of FSP27 with CIDEA resulted in diminished levels of FSP27 protein compared with that seen when FSP27 alone is expressed. Because CIDEA has been reported to be a short-lived protein, it is possible that since FSP27 can complex with CIDEA, this may contribute to the

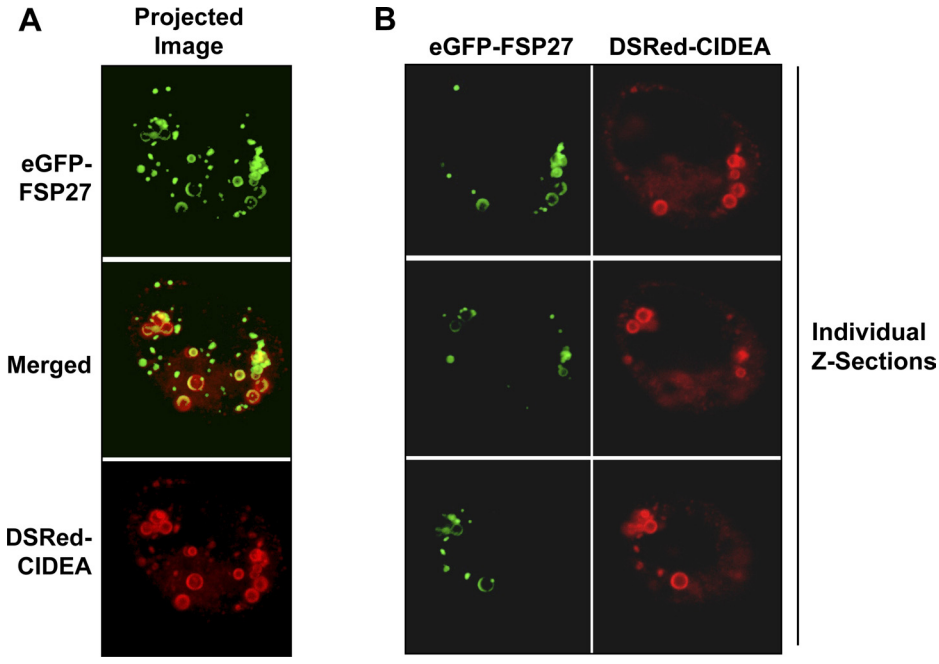

Fig. 10. FSP27 and CIDEA colocalize on small and large lipid droplets. HeLa cells were incubated for 2 days with 400 μM BSA-complexed OA to induce lipid droplet formation. Cells were then cotransfected with full-length fluorescent protein fusion expression constructs for FSP27 (eGFP-FSP27) and CIDEA (DSRed-CIDEA) and observed at 14 h posttransfection with confocal microscopy. *A*: projected images of all Z-sections are shown, with *top* and *bottom* depicting signal for eGFP-FSP27 and DSRed-CIDEA, respectively. Merged image for eGFP-FSP27 and DSRed-CIDEA is shown in the *middle*. *B*: individual Z-sections. Three representative Z-sections (*top*, *middle*, and *bottom*) are shown. Signals for eGFP-FSP27 and DSRed-CIDEA are shown in the *right* and *left* sets, respectively.

reduced steady-state level of FSP27 of protein we observed, possibly through effects on FSP27 protein half-life.

To address this, we utilized the protein synthesis inhibitor cycloheximide and used Western blot analysis to assess levels of FSP27 protein in the absence and presence of CIDEA protein expression in transfected 293T cells, a cell type previously employed in studies of CIDEA protein stability (4). As shown in Fig. 9*B*, *left*, and in the accompanying graph of FSP27 protein half-life measurements in Fig. 9*C*, *left*, we find that FSP27 protein has a half-life of ~1.3 h. Figure 9*B*, *middle*, and the accompanying graph in Fig. 9*C*, *right*, reveal that protein half-life of FSP27 is moderately reduced to ~1 h in the presence of CIDEA coexpression. The Western blot in Fig. 9*B*, *right*, compares the steady-state level of FSP27 in the absence and presence of CIDEA, used as the *time 0* point in the cycloheximide treatment study, and is consistent with our observations in Fig. 9*A*. Quantification of the steady-state signal for FSP27 protein in the absence and presence of CIDEA indicates a 36% reduction of FSP27 protein level in the presence of CIDEA. This is consistent with the degree of effect we note for reduction of FSP27 half-life by CIDEA expression.

The biological consequence of interaction of FSP27 and CIDEA remains to be investigated. Because these proteins interact with each other, the possibility exists that they may each also interact with similar or the same subset of partner proteins at lipid droplets. Studies with the PAT lipid droplet protein family, the first and to date the best-studied group of lipid droplet-associated proteins, which includes perilipin, adipophilin, and TIP47 (2, 3, 7, 22, 39, 40), have revealed that specific PAT proteins are preferentially and/or exclusively associated with differing sizes of nascent through large lipid droplets within a single cell (2, 7). It has also been reported that expression of certain PAT proteins can cause the loss of lipid droplet association of other PAT proteins (22, 39). These observations support a working model for exchangeable PAT proteins in the structure, function, and dynamic nature of lipid droplets. To begin to address the association of FSP27 and CIDEA among lipid droplets within a single cell, we examined distribution of these proteins using transient transfection of lipid-loaded HeLa cells utilizing a 1:1 ratio of eGFP-FSP27 and DSRed-CIDEA to test for either colocalization or mutual exclusivity. As shown by the confocal analysis in Fig. 10, we find that, within single cells, both FSP27 and CIDEA are colocalized on the full size range of cellular lipid droplets. Although the projected image in Fig. 10*A* appears to show some enrichment of FSP27 at smaller lipid droplets, and CIDEA at larger droplets, close inspection of the individual Z-sections for either eFGP-FSP27 or DSRed-CIDEA signal, shown in Fig. 10*B*, indicates that all evident lipid droplets show evidence of association of both FSP27 and CIDEA. In addition, FSP27 and CIDEA are colocalized in all other regions within the cells; these are presumably very tiny lipid droplets/deposits that do not yet have the evident, clearly circular morphology of discernable lipid droplets. Thus, unlike observations for particular PAT proteins, the two CIDE family proteins we tested, FSP27 and CIDEA, fail to demonstrate any degree of mutual exclusivity with respect to their association with varying size lipid droplets. Although the interplay between FSP27, CIDEA, and lipid droplets remains to be more fully explored, our observations suggest that FSP27 cannot effectively displace CIDEA, nor vice versa.

In conclusion, FSP27 has dual functions as a lipid droplet protein in cellular lipid metabolism and as a robust proapoptotic factor (12, 13, 25). Our studies are the first to demonstrate interaction of CIDEA and FSP27 and that this interaction likely involves the FSP27 CIDE C domain. To our knowledge, only a single study to date has addressed a potential functional interaction for FSP27 and CIDEA, albeit in an indirect manner. It was reported that in cultured brown adipocytes siRNA-mediated depletion of FSP27 had no apparent effects on CIDEA localization to the lipid droplet surface (26). However, our findings raise the possibility that CIDEA and FSP27 may work synergistically via heterodimerization in regard to certain aspects of adipocyte metabolism and/or lipid droplet function. Our data also suggest that, in studies addressing the role of FSP27 or CIDEA in cells where both proteins exist, for example, human white adipocytes, the impact of dimerization of FSP27 and CIDEA should be considered when the respective functional roles of these proteins are assessed.

It is currently not clear whether the proapoptotic effect of FSP27 is merely a functional remnant of its evolutionary relationship with the major apoptotic nuclease DFF40/DFF45 (41). However, it is intriguing that we demonstrate that the proapoptotic function and lipid droplet localization function of FSP27 requires a subregion of its CIDE C domain, a protein motif that is unique to the three CIDE family members (FSP27, CIDEA, and CIDEB) and not present in DFF40/DFF45 (11, 41). In adipocytes wherein a high degree of lipolysis occurs, lipid droplet content is diminished. The prolipolytic agent TNFα results in loss of lipid content and diminution of transcript expression for a large number of adipocyte-expressed genes and can induce adipocyte apoptosis (28–30). It is not currently known whether a portion of the lipid droplet proteome becomes released from the lipid droplet milieu as a result of TNFα-induced or other lipolysis. One can speculate that these "freed" lipid droplet proteins might be involved in various events to impact or initiate intracellular signaling pathways. These may function to communicate the status of cellular triacylglycerol energy stores, and by extension the overall health of the adipocyte, to other organelles within the cell.

ACKNOWLEDGMENTS

We thank Dr. H. F. Ding (Medical College of Georgia) for the dominant negative caspase-9 expression construct.

GRANTS

This work is supported by an institutional grant from the University of Toledo College of Medicine.

DISCLOSURES

No conflicts of interest are declared by the author(s).

REFERENCES

1. **Badman MK, Flier JS.** The adipocyte as an active participant in energy balance and metabolism. *Gastroenterology* 132: 2103–2115, 2007.
2. **Bickel PE, Tansey JT, Welte MA.** PAT proteins, an ancient family of lipid droplet proteins that regulate cellular lipid stores. *Biochim Biophys Acta* 1791: 419–440, 2009.
3. **Brasaemle DL.** Thematic review series: adipocyte biology. The perilipin family of structural lipid droplet proteins: stabilization of lipid droplets and control of lipolysis. *J Lipid Res* 48: 2547–2559, 2007.

4. **Chan SC, Lin SC, Li P.** Regulation of Cidea protein stability by the ubiquitin-mediated proteasomal degradation pathway. *Biochem J* 408: 259–266, 2007.
5. **Chen Z, Guo K, Toh SY, Zhou Z, Li P.** Mitochondria localization and dimerization are required for CIDE-B to induce apoptosis. *J Biol Chem* 275: 22619–22622, 2000.
6. **Ding HF, Lin YL, McGill G, Juo P, Zhu H, Blenis J, Yuan J, Fisher DE.** Essential role for caspase-8 in transcription-independent apoptosis triggered by p53. *J Biol Chem* 275: 38905–38911, 2000.
7. **Ducharme NA, Bickel PE.** Lipid droplets in lipogenesis and lipolysis. *Endocrinology* 149: 942–949, 2008.
8. **Erdtmann L, Franck N, Lerat H, Le Seyec J, Gilot D, Cannie I, Gripon P, Hibner U, Guguen-Guillouzo C.** The hepatitis C virus NS2 protein is an inhibitor of CIDE-B-induced apoptosis. *J Biol Chem* 278: 18256–18264, 2003.
9. **Flier JS.** Obesity wars: molecular progress confronts an expanding epidemic. *Cell* 116: 337–350, 2004.
10. **Granneman JG, Moore HP.** Location, location: protein trafficking and lipolysis in adipocytes. *Trends Endocrinol Metab* 19: 3–9, 2008.
11. **Inohara N, Koseki T, Chen S, Wu X, Nunez G.** CIDE, a novel family of cell death activators with homology to the 45 kDa subunit of the DNA fragmentation factor. *EMBO J* 17: 2526–2533, 1998.
12. **Keller P, Petrie JT, De Rose P, Gerin I, Wright WS, Chiang SH, Nielsen AR, Fischer CP, Pedersen BK, MacDougald OA.** Fat-specific protein 27 regulates storage of triacylglycerol. *J Biol Chem* 283: 14355–14365, 2008.
13. **Kim JY, Liu K, Zhou S, Tillison K, Wu Y, Smas CM.** Assessment of fat-specific protein 27 in the adipocyte lineage suggests a dual role for FSP27 in adipocyte metabolism and cell death. *Am J Physiol Endocrinol Metab* 294: E654–E667, 2008.
14. **Li JZ, Li P.** Cide proteins and the development of obesity. *Novartis Found Symp* 286: 155–159; discussion 159–163, 196–203, 2007.
15. **Li JZ, Ye J, Xue B, Qi J, Zhang J, Zhou Z, Li Q, Wen Z, Li P.** Cideb regulates diet-induced obesity, liver steatosis, and insulin sensitivity by controlling lipogenesis and fatty acid oxidation. *Diabetes* 56: 2523–2532, 2007.
16. **Li P.** Cidea, brown fat and obesity. *Mech Ageing Dev* 125: 337–338, 2004.
17. **Liang L, Zhao M, Xu Z, Yokoyama KK, Li T.** Molecular cloning and characterization of CIDE-3, a novel member of the cell-death-inducing DNA-fragmentation-factor (DFF45)-like effector family. *Biochem J* 370: 195–203, 2003.
18. **Liu P, Ying Y, Zhao Y, Mundy DI, Zhu M, Anderson RG.** Chinese hamster ovary K2 cell lipid droplets appear to be metabolic organelles involved in membrane traffic. *J Biol Chem* 279: 3787–3792, 2004.
19. **Lugovskoy AA, Zhou P, Chou JJ, McCarty JS, Li P, Wagner G.** Solution structure of the CIDE-N domain of CIDE-B and a model for CIDE-N/CIDE-N interactions in the DNA fragmentation pathway of apoptosis. *Cell* 99: 747–755, 1999.
20. **Matsusue K, Kusakabe T, Noguchi T, Takiguchi S, Suzuki T, Yamano S, Gonzalez FJ.** Hepatic steatosis in leptin-deficient mice is promoted by the PPARgamma target gene Fsp27. *Cell Metab* 7: 302–311, 2008.
21. **Nishino N, Tamori Y, Tateya S, Kawaguchi T, Shibakusa T, Mizunoya W, Inoue K, Kitazawa R, Kitazawa S, Matsuki Y, Hiramatsu R, Masubuchi S, Omachi A, Kimura K, Saito M, Amo T, Ohta S, Yamaguchi T, Osumi T, Cheng J, Fujimoto T, Nakao H, Nakao K, Aiba A, Okamura H, Fushiki T, Kasuga M.** FSP27 contributes to efficient energy storage in murine white adipocytes by promoting the formation of unilocular lipid droplets. *J Clin Invest* 118: 2808–2821, 2008.
22. **Orlicky DJ, Degala G, Greenwood C, Bales ES, Russell TD, McManaman JL.** Multiple functions encoded by the N-terminal PAT domain of adipophilin. *J Cell Sci* 121: 2921–2929, 2008.
24. **Puri V, Czech MP.** Lipid droplets: FSP27 knockout enhances their sizzle. *J Clin Invest* 118: 2693–2696, 2008.
25. **Puri V, Konda S, Ranjit S, Aouadi M, Chawla A, Chouinard M, Chakladar A, Czech MP.** Fat-specific protein 27, a novel lipid droplet protein that enhances triglyceride storage. *J Biol Chem* 282: 34213–34218, 2007.
26. **Puri V, Ranjit S, Konda S, Nicoloro SM, Straubhaar J, Chawla A, Chouinard M, Lin C, Burkart A, Corvera S, Perugini RA, Czech MP.** Cidea is associated with lipid droplets and insulin sensitivity in humans. *Proc Natl Acad Sci USA* 105: 7833–7838, 2008.
27. **Qi J, Gong J, Zhao T, Zhao J, Lam P, Ye J, Li JZ, Wu J, Zhou HM, Li P.** Downregulation of AMP-activated protein kinase by Cidea-mediated ubiquitination and degradation in brown adipose tissue. *EMBO J* 27: 1537–1548, 2008.
28. **Ruan H, Hacohen N, Golub TR, Van Parijs L, Lodish HF.** Tumor necrosis factor-alpha suppresses adipocyte-specific genes and activates expression of preadipocyte genes in 3T3-L1 adipocytes: nuclear factor-kappaB activation by TNF-alpha is obligatory. *Diabetes* 51: 1319–1336, 2002.
29. **Ruan H, Lodish HF.** Insulin resistance in adipose tissue: direct and indirect effects of tumor necrosis factor-alpha. *Cytokine Growth Factor Rev* 14: 447–455, 2003.
30. **Ruan H, Miles PD, Ladd CM, Ross K, Golub TR, Olefsky JM, Lodish HF.** Profiling gene transcription in vivo reveals adipose tissue as an immediate target of tumor necrosis factor-alpha: implications for insulin resistance. *Diabetes* 51: 3176–3188, 2002.

30a **Rubio-Cabezas C, Puri V, Murano I, Saudek V, Semple RK, Dash S, Hyden CS, Bottomley W, Vigouroux C, Magré J, Raymond-Barker P, Murgatroyd PR, Chawla A, Skepper JN, Chatterjee VK, Suliman S, LD Screening Consortium, Patch AM, Agarwal AK, Garg A, Barroso I, Cinti S, Czech MP, Argente J, O'Rahilly S, Savage DB.** Partial lipodystrophy and insulin resistant diabetes in a patient with a homozygous nonsense mutation in CIDEC. *EMBO Molecular Medicine* 1: 280–287, 2009.

31. **Smirnova E, Goldberg EB, Makarova KS, Lin L, Brown WJ, Jackson CL.** ATGL has a key role in lipid droplet/adiposome degradation in mammalian cells. *EMBO Rep* 7: 106–113, 2006.
32. **Srinivasula SM, Ahmad M, Fernandes-Alnemri T, Alnemri ES.** Autoactivation of procaspase-9 by Apaf-1-mediated oligomerization. *Mol Cell* 1: 949–957, 1998.
33. **Toh SY, Gong J, Du G, Li JZ, Yang S, Ye J, Yao H, Zhang Y, Xue B, Li Q, Yang H, Wen Z, Li P.** Up-regulation of mitochondrial activity and acquirement of brown adipose tissue-like property in the white adipose tissue of fsp27 deficient mice. *PLoS ONE* 3: e2890, 2008.
34. **Unger RH.** Lipotoxic diseases. *Annu Rev Med* 53: 319–336, 2002.
35. **Unger RH.** Minireview: weapons of lean body mass destruction: the role of ectopic lipids in the metabolic syndrome. *Endocrinology* 144: 5159–5165.
36. **Unger RH.** The physiology of cellular liporegulation. *Annu Rev Physiol* 65: 333–347, 2003.
37. **Unger RH, Orci L.** Lipotoxic diseases of nonadipose tissues in obesity. *Int J Obes Relat Metab Disord* 24, *Suppl* 4: S28–S32, 2000.
38. **Walther TC, Farese RV Jr.** The life of lipid droplets. *Biochim Biophys Acta* 1791: 459–466, 2009.
39. **Wolins NE, Brasaemle DL, Bickel PE.** A proposed model of fat packaging by exchangeable lipid droplet proteins. *FEBS Lett* 580: 5484–5491, 2006.
40. **Wolins NE, Quaynor BK, Skinner JR, Schoenfish MJ, Tzekov A, Bickel PE.** S3–12, Adipophilin, and TIP47 package lipid in adipocytes. *J Biol Chem* 280: 19146–19155, 2005.
41. **Wu C, Zhang Y, Sun Z, Li P.** Molecular evolution of Cide family proteins: novel domain formation in early vertebrates and the subsequent divergence. *BMC Evol Biol* 8: 159, 2008.
42. **Ye J, Li JZ, Liu Y, Li X, Yang T, Ma X, Li Q, Yao Z, Li P.** Cideb, an ER- and lipid droplet-associated protein, mediates VLDL lipidation and maturation by interacting with apolipoprotein B. *Cell Metab* 9: 177–190, 2009.
43. **Zechner R, Kienesberger PC, Haemmerle G, Zimmermann R, Lass A.** Adipose triglyceride lipase and the lipolytic catabolism of cellular fat stores. *J Lipid Res* 50: 3–21, 2009.
44. **Zhou Z, Yon Toh S, Chen Z, Guo K, Ng CP, Ponniah S, Lin SC, Hong W, Li P.** Cidea-deficient mice have lean phenotype and are resistant to obesity. *Nat Genet* 35: 49–56, 2003.